Research Square

Preprints are preliminary reports that have not undergone peer review.
They should not be considered conclusive, used to inform clinical practice,
or referenced by the media as validated information.

Irrigation-induced precipitation as a water externality of agricultural production

Elena De Petrillo

elena.depetrillo@polito.it

Politecnico di Torino https://orcid.org/0000-0001-7398-5742

Francesco Laio

Politecnico di Torino

Luca Ridolfi

Politecnico di Torino

Marta Tuninetti

Polytechnic University of Turin https://orcid.org/0000-0003-2619-8783

Article

Keywords:

Posted Date: November 12th, 2026

DOI: https://doi.org/10.21203/rs.3.rs-11452819/v1

License: This work is licensed under a Creative Commons Attribution 4.0 International License.
Read Full License

Additional Declarations: There is **NO** Competing Interest.

Irrigation-induced precipitation as a water externality of agricultural production

Elena De Petrillo[1*], Francesco Laio[1], Luca Ridolfi[1], Marta Tuninetti[1]

[1*]Department of Environment, Land and Infrastructure Engineering, Politecnico di Torino, c.so Duca degli Abruzzi 24, Turin, 10129, Italy.

*Corresponding author(s). E-mail(s): elena.depetrillo@polito.it;

Abstract

Irrigation water lost through evapotranspiration is redistributed globally: physically, via atmospheric moisture transport and downwind precipitation, and virtually, embedded in traded crops. These pathways have traditionally been studied independently, leaving it unclear whether irrigation-induced atmospheric recycling compensates for or amplifies irrigation water use for food production and trade. By coupling agro-hydrological modeling of 148 crops with country-to-country atmospheric moisture transport and international trade data, we find that 72% of irrigation-induced evapotranspiration returns to land as precipitation (the remainder being lost to oceans), with 45% crossing national borders through the atmosphere, more than three times the volume redistributed through virtual water trade. Rather than offsetting trade-based dependencies, atmospheric transfers largely reinforce them: 73% of countries hold the same role in both networks, as net donors or net recipients. Water dependencies between countries therefore extend beyond trade to the atmosphere, an externality that current water governance and food security assessments fail to capture.

Keywords: irrigation-induced precipitation recycling, virtual water trade, water footprint, transboundary networks

Global food demand and increasingly affluent societies have made the food system the major forcing shaping hydrological pressures [1, 2]: irrigated land, about 20% of global cropland, supplies about 40% of global agricultural output, while agriculture accounts for 72% of global freshwater withdrawals [3]. About half of the water withdrawn for agriculture (blue water) returns to the atmosphere through evapotranspiration, the

remainder flowing back to rivers and aquifers via return flow and deep percolation [4]. The evaporated moisture can travel long distances before precipitating [5], sustaining rainfed production as green water flow [6]. This atmospheric recycling via the evaporation-precipitation cycle on land is substantial: total land evapotranspiration (including the contribution from irrigation) contributes 40–45% of global terrestrial precipitation [7, 8]. Irrigation-induced evapotranspiration volume, also referred to as irrigation consumptive water use [4], corresponds to the blue water footprint (WF_b) of agricultural production. Through trade, the WF_b is virtually transferred to consumption regions [9], generating a blue virtual water trade (VWT) that links production to consumption [10]. This is fundamental since about one-quarter of globally produced food calories are traded internationally [11], and the volume of traded agricultural goods has more than doubled over the past three decades [12].

So far, two parallel bodies of literature have explored the hydrological implications of irrigation-induced evapotranspiration. The first one examines how VWT redistributes irrigation water use across countries, together with the associated water savings, pressure, and stress [13–17]. The second one follows irrigation-induced evapotranspiration through the atmosphere, tracing where it precipitates and how it feeds back on climate, from local to global scales [18–22]. Despite some studies proposing the integration of atmospheric recycling into basin-scale water-use assessment [23–25], these two fields have evolved largely independently. As a result, we lack an integrated picture of how irrigation water used for agricultural production is redistributed among countries, both both physically and economically.

It therefore remains unclear whether atmospheric recycling offsets or reinforces the water dependencies created by trade of irrigated agricultural production. Recent work has begun to connect atmospheric moisture flows with trade: Pranindita et al. [26] traced moisture from forests transpiration to precipitation over crop production and, subsequently, exports, showing that crop producers, exporters and importers all depend on upwind forested countries; Fahrlander et al. [27] coupled total, rather than irrigation-specific, atmospheric moisture flow from land and virtual water trade networks through a triadic feed-forward framework, identifying critical moisture-to-trade mediator countries and a wealth-related asymmetry in nations' net position. Both studies trace dependencies that chain atmospheric and trade links across several countries, but neither isolates irrigation, the component of evapotranspiration that is directly managed through infrastructures. The direct balance between the irrigation water that each country exchanges through the atmosphere and through trade therefore remains unknown. Here we quantify this balance for 162 countries by coupling agro-hydrological modeling of 148 crops with bilateral atmospheric moisture transport and international trade data.

Specifically, we assess (i) how much irrigation-induced evapotranspiration returns to land as downwind precipitation, highlighting the crossing of national borders, (ii) the extent to which these atmospheric transfers offset each country's consumptive water use for irrigated agriculture, and (iii) whether atmospheric flows reinforce or attenuate the net exporter and net importer roles that countries hold in VWT.

We use the waterCROP model [28] to estimate blue water demand for 148 crops, integrate VWT data from the CWASI database [29, 30] to link production to consumption countries, and combine these with cross-border atmospheric moisture connections from the RECON dataset [31]—a cell-scale atmospheric moisture connection dataset based on the Lagrangian tracking model UTrack [32, 33] and constrained by ERA5 reanalysis to ensure consistency in the annual hydrological balance [34].

We find that most irrigation-induced evapotranspiration returns to land as precipitation, and that the atmosphere moves roughly three times more irrigation water across national borders than crop trade does. Rather than offsetting the dependencies created by trade, these atmospheric transfers largely reinforce them, as most countries hold the same net donor or recipient role in both networks. Beyond mapping these transboundary links, we assess how far the irrigation water a country exports through the atmosphere offsets blue consumptive water use elsewhere. Together, these results show that water-use accounting and VWT analyses alone miss a substantial share of the transboundary externalities of irrigated agriculture.

1 Main

1.1 The atmosphere moves more irrigation water across borders than trade

Globally, irrigation-induced evapotranspiration amounts to 1,052 km^3 yr^{-1}, comparable to the annual discharge of the Yangtze River, from 3.6 million km^2 of irrigated land, an area similar to that of India. Of this volume, 72% (752 km^3 yr^{-1}) returns to land as precipitation, peaking in India, Bhutan, Nepal and Bangladesh (44–154 mm yr^{-1}); and the remaining 28% (299 km^3 yr^{-1}) precipitates over the oceans (Figs. 1, Extended Data 1).

The irrigation-induced evaporation recycling is higher than the typical global land evaporation recycling, [7, 31, 33], consistent with the concentration of irrigated land in continental interiors and downwind of large land masses, particularly in South and Central Asia, where evaporated moisture is more likely to precipitate over land before reaching the ocean.

However, about 30% of countries exceed 50% loss to the oceans (e.g., >90% in New Zealand and Costa Rica, 83% in Japan, and 69% in Australia; Fig. Extended Data 1), whereas domestic irrigation recycling (DIR) exceeds 50% only in a handful of countries (Fig.Extended Data 2).

Among the four countries with the largest use of irrigation water (or blue water footprint, WF_b), only China recycles domestically more than half of its irrigation (58%), whereas the USA, India, and Pakistan recycle 37%, 29%, and 18.5%, respectively, and therefore send most of their irrigation-induced moisture abroad or over the oceans (Fig. 1).

About 45% of global irrigation-induced evapotranspiration (476 km^3 yr^{-1}) crosses national borders through the atmosphere (contributing around 10% of total land-generated precipitation for several countries, Fig.Extended Data 4), more than three times the 13% (134 km^3 yr^{-1}) embedded in internationally traded crops (i.e., the blue VWT).

The USA, India, and Pakistan are, in fact, the next exporters of irrigation-induced moisture, together with Egypt and Iran (net exports of 14.5–82 $km^3\ yr^{-1}$), followed by Uzbekistan, Sudan, Thailand, Spain, and approximately 50 other countries. Conversely, about 60% of the 162 irrigated countries are net atmospheric importers, led by China (109 $km^3\ yr^{-1}$) and Russia (49 $km^3\ yr^{-1}$).

How irrigation water is partitioned among these transboundary pathways varies widely between countries. Taken together, both networks originate from sourcing clusters, but they differ in structure. As shown in Fig.1), the atmospheric network is dense and regional, shaped by the locations of irrigated areas, concentrated in South and Central Asia, the Mediterranean, the Arabian Peninsula, and North America. The virtual water network, shaped by both irrigation equipment and socioeconomic ties, is sparser and reaches farther, connecting countries up to tens of thousands of kilometers apart.

This analysis shows how these two networks can reveal transboundary links that remain hidden in trade-based accounting. Egypt, for example, is the third-largest net atmospheric exporter: it exports irrigation-induced moisture equivalent to 34 $mm\ yr^{-1}$ over its territory, nearly twice its total annual precipitation (18 $mm\ yr^{-1}$), yet receives only 0.1% of this volume back as irrigation-induced precipitation from other countries and about 4% as blue virtual water imports. Much of this moisture instead reaches sub-Saharan Africa: Egyptian irrigation supplies 47% of the cross-border irrigation-induced precipitation received by Ethiopia and 42% of that received by Nigeria. The link with Ethiopia runs opposite to the Nile, whose upstream flow sustains Egyptian irrigation, adding an atmospheric dimension to one of the most contested transboundary water relationships.

1.2 Irrigated areas drive blue water redistribution to different beneficiaries through the atmosphere and trade

Irrigation water can leave a country in two ways: as moisture that precipitates in another country and as virtual water embedded in exported crops. A country that transfers water to the same partner through both pathways gives up both the water and the crops produced with it, while earning revenue from their sale (amplifying transfer). When the two flows run in opposite directions, water sent through one pathway is partly returned through the other (attenuating transfer). To assess which case prevails, we compare the structure of the two networks and their dominant countries, then examine the direction of bilateral flows and the distances over which they are comparable in magnitude (Fig. 2).

Both networks show a strong in–out strength asymmetry: the top 30 sources of irrigation-induced moisture account for 92% of cross-border atmospheric transport, and the top 30 blue virtual water exporters for 90% of global exports (Fig. 2a,b). Imports are more evenly distributed, particularly in trade, where the top 30 importers account for 67% of the total (86% in the atmospheric network).

Few countries act in series between the two networks, receiving irrigation water through the atmosphere and passing it on through trade: only 13 countries appear among both the top 30 atmospheric importers and the top 30 blue virtual water

exporters, together receiving 52% of cross-border irrigation-induced precipitation and supplying 64% of global exports.

India dominates the atmospheric network, exporting 130 km^3 yr^{-1} of irrigation-induced moisture (27% of the global cross-border volume), more than half of which reaches China (Fig. 2a). The USA dominates trade instead: it is the largest blue virtual water exporter (24 km^3 yr^{-1}, 18% of the global volume), supplying 197 countries, yet even its largest link, USA→China (4.2 km^3 yr^{-1}), is an order of magnitude smaller than the flows received by the RoW (39 km^3 yr^{-1}, 29% of global trade), the largest destination of the network (Fig. 2b). China is in fact the main importer in both networks, receiving a total of 129 km^3 yr^{-1} of irrigation-induced precipitation and 13 km^3 yr^{-1} of blue virtual water. Pakistan is the second-largest source of irrigation-induced moisture (63 km^3 yr^{-1}) and the third-largest blue virtual water exporter (15 km^3 yr^{-1}), after the USA and India (21 km^3 yr^{-1}).

Major irrigating countries indeed move up from the atmospheric import to the trade export ranking (solid lines in Fig. 2): the USA (from 21st to 1st), Thailand (23rd to 5th), Turkmenistan (29th to 14th), Uzbekistan (22nd to 13th), Pakistan (9th to 3rd), and Iran (13th to 9th). Conversely, large recipients of irrigation-induced precipitation move down (dotted lines): China drops from 1st to 26th, exporting only 0.9 km^3 yr^{-1} of blue virtual water (less than 1% of its WF_b), followed by Afghanistan (11th to 25th) and Kazakhstan (7th to 18th).

These shifts reflect how bilateral links may relate in the two networks. Of the roughly 300 links that carry 90% of cross-border atmospheric transport and 70% of blue virtual water trade, 75 transfer water in the same directions in the two networks. These amplifying links carry half of atmospheric moisture and 26% of virtual water trade. Only 38 links are reciprocal, with blue virtual water flowing back to the country where the irrigation-induced moisture originated, and they carry 14% of atmospheric transport and 18% of virtual water trade. Amplifying transfers therefore move more than three times as much atmospheric volume as attenuating ones.

This dominance reflects the geography of irrigation. The largest irrigated regions, particularly in South Asia, lie upwind of populous neighbors that also import their crops, so the same partners receive irrigation water both as precipitation and as food. For these importers, dependence on the exporting country is compounded rather than diversified: a contraction of irrigation in the source country, for example due to groundwater depletion or drought, would reduce both pathways at once, and export restrictions would remove only one of them.

Reciprocal links can partly balance these transfers, but only in a few pairs are the two flows of similar magnitude. These include neighbors with strong two-way agricultural trade, such as Mexico and the USA (3.3 and 3.0 km^3 yr^{-1}), Bangladesh and India (3.8 and 2.2 km^3 yr^{-1}), and Brazil and Argentina (0.6 km^3 yr^{-1} in both directions), as well as India and more distant partners such as Sudan and Saudi Arabia (0.5–0.9 km^3 yr^{-1}, 3,500–5,200 km apart). In these cases, irrigation water exchanged through the atmosphere and trade creates mutual, rather than one-directional, dependence, which could provide a basis for bilateral water accounting beyond trade alone.

Whether these concordant or reciprocal flows can actually balance is further constrained by their size and distance: atmospheric volume concentrates on a few large

regional flows, whereas virtual water trade spreads over many smaller links (Fig. 2c; Extended Data Fig. Extended Data 5a). Flow-weighted averages are 2,570 km for atmospheric flows and 5,490 km for virtual water, and less than 0.1% of the atmospheric volume travels beyond 10,000 km, against 19% of the blue virtual water volume (Fig. 2e; Extended Data Fig. Extended Data 5b). The two flows can potentially balance within a country pair only between 3,000 and 6,000 km, in both the concordant and reciprocal directions (Extended Data Fig. Extended Data 6). Summed over all partners, these bilateral relations determine each country's net position in the two networks, and whether its role is amplified or attenuated from one network to the other.

1.3 Most countries hold the same net role in the atmospheric and trade networks

The bilateral links examined above describe how irrigation water moves between pairs of countries. Here we sum these flows over all partners to determine each country's net position in each network, whether it is a net exporter or net importer of irrigation water, and whether it holds the same role in both (Fig.3). Because concordant links dominate, most countries (73%) play the same role in both networks, while the remaining 27% switch roles from one network to the other.

Since irrigated areas are quite concentrated globally, the two networks are particularly aligned on the export side: irrigation-induced atmospheric and blue virtual water exports are strongly correlated (Pearson's $r = 0.78$ on log-transformed volumes, and $r = 0.71$ in mm; Figs. Extended Data 7a and Extended Data 8a). Countries that are net exporters in both networks (19%) hold 67% of the global WF_b and carry the largest volumes, accounting for 74% of cross-border irrigation-induced atmospheric exports and 81% of blue virtual water exports: India, Pakistan, Iran, Egypt, and the USA occupy the extreme export volumes in both networks (Fig.3b). These countries support irrigated production, while others benefit from additional irrigation-induced precipitation and irrigation savings from imported food. Overall, most countries (54%) are net importers in both networks, with Europe, Sub-Saharan Africa, and East Asia dominating. They fall into two groups: wealthy food importers with little irrigation, such as Japan, Germany, and the United Kingdom, and large countries downwind of major WF_b countries, such as China, Russia, and Ethiopia. Both depend on water-use decisions elsewhere, and would be affected through both pathways if irrigation upwind or in exporting countries declined. The group receives 68% of cross-border irrigation-induced precipitation and 54% of blue virtual water imports.

In role-switching countries (27% of the total), one network partly compensates the other, meaning these countries attenuate their role to other countries through either the atmospheric (olive down-rightward arrows) or virtual water (purple up-leftward arrows) networks.

Twelve countries fall into the first case, benefiting from precipitation generated by irrigation in foreign countries while exporting agricultural products, so part of the water received through the atmosphere may indirectly attenuate the irrigation needs of blue virtual water trade. These countries are mostly in Latin America and

Central Asia (e.g., Argentina, Peru, Bolivia, Kazakhstan, Kyrgyzstan, Tajikistan, and Ukraine), key hubs of global food supplies.

Conversely, the opposite attenuation — where blue virtual water trade buffers the atmospheric irrigation-induced water they send to other countries through the atmosphere—occurs in 32 countries, mainly water-scarce countries in North Africa and West Asia, such as Saudi Arabia and Iraq, which absorb 26% of global blue virtual water imports with 9% of the global WF_b. Further cases are Bangladesh, Mexico, Venezuela, Nigeria, Turkey, and Italy.

Because atmospheric roles are set by geography and circulation, whereas trade roles reflect economic structure and socioeconomic drivers, role switching identifies where physical and economic water exchanges can attenuate atmospheric or economic water externalities.

1.4 The magnitude of cross-border irrigation-induced precipitation compares with national blue water footprints

To evaluate the relative impact of cross-border irrigation-induced precipitation flows, Fig. 4 normalizes net atmospheric import and export by each country's WF_b, so that countries with very different irrigation volumes can be compared: the benefit ratio (IAW/WF_b), i.e., the irrigation-induced precipitation received from other countries relative to the national WF_b, and the contribution ratio (EAW/WF_b), i.e., the share of the national WF_b exported to other countries as moisture.

Normalization shows how large these flows are relative to national blue water use: the median country exports as moisture 57% of its WF_b and receives from abroad irrigation-induced precipitation equivalent to 78% of it. Among the 25 countries with the largest WF_b, 15 export at least half of their WF_b to other countries as moisture. The exceptions are represented by countries that emerge as net atmospheric importers (Fig. 3), led by China, whose benefit ratio approaches 1 (0.93), mostly owing to precipitation originating in India (Fig. 2), whereas its contribution ratio is only 0.14, given its high domestic recycling and loss to the ocean (Figs. Extended Data 2 and Extended Data 1). Indonesia and Argentina follow the same pattern with smaller volumes, whereas Vietnam, Afghanistan and Kazakhstan export a large share of their WF_b (contribution ratios of 0.42–0.81) but receive even more irrigation-induced precipitation from neighboring countries.

On the receiving side, 46% of irrigated countries receive from foreign irrigation at least as much water as they consume for their own irrigated production as WF_b (benefit ratio ≥ 1). Together, they receive 42% of cross-border irrigation-induced precipitation while holding only 4% of global WF_b. Thirteen of them have a WF_b above 1 $km^3\ yr^{-1}$, with remarkable examples of Tajikistan, one of the largest recipients of irrigation-induced precipitation (Fig. 1), Ukraine and Kazakhstan, which are net blue virtual water exporters, and France, a net importer in both networks. The most extreme values ($\gg$10) mostly occur in countries that combine a small WF_b with a substantial contribution from regional irrigation-induced precipitation recycling (Fig. Extended Data 9).

This analysis shows that irrigation-induced precipitation contributes to agriculture not only domestically but also across borders, and its magnitude compares with

national blue water footprints for several countries. This mechanism is particularly relevant when considered alongside water scarcity metrics and the socio-economic opportunity cost of trade.

2 Discussion

Over the past two decades, virtual water research has reconceptualized the global water cycle by accounting for the water embedded in traded crops [10], introducing a global dimension to water governance [35]: trade can relieve water-scarce importers [9], but often burdens developing exporters facing economic or physical water scarcity [14, 15, 17]. Evidence on its dynamics [36], hydrological impacts [13, 14, 16], and socio-economic drivers [37–39] now informs trade, agricultural policies, and global water risk assessments [14, 15, 17].

This study shows that atmospheric recycling of irrigation-induced evapotranspiration is another key component for capturing socio-hydrological relationships between countries. Transboundary lake and river basins account for an estimated 60% of global freshwater flow [40]; similarly, 45% of the global WF_b crosses national borders through the atmosphere, more than three times the share redistributed through international trade (13%) (Figs. 1 and 2).

Despite irrigation being highly concentrated—42 countries account for 95% of the global WF_b, and the four largest for 60%—irrigated countries can play heterogeneous roles in redistributing water across countries. One in five countries exports irrigation water through both pathways, as irrigation-induced moisture and as traded irrigated crops; together, these countries account for 67% of global WF_b. Their irrigation therefore affects most countries (54%), which import through both pathways, through both rainfall and imported food. The remaining 27% of countries are net exporters in one network and net importers in the other, so that a net outflow through one is partly offset by a net inflow through the other. For example, water-scarce countries export moisture but import virtual water, whereas food exporters export virtual water but receive irrigation-induced precipitation. Normalizing by national WF_b further reveals a mismatch between where irrigation water is consumed and where its atmospheric benefits accrue: most countries (61%) receive more irrigation-induced precipitation than they export, yet hold only 23% of global WF_b, whereas the few net exporters consume the remaining 77%, bearing the water use that sustains precipitation elsewhere. Because atmospheric and trade flows are most comparable between countries 3,000–6,000 km apart (Fig. Extended Data 6), this mismatch is most likely to be rebalanced at the regional to continental scale, where cooperation between neighboring countries can account for both pathways.

Because different drivers shape how the two networks propagate water flows, they offer different levers to modify a country's net compounded balance. The net atmospheric exchange depends mainly on where irrigation is located, since the siting of irrigated areas relative to prevailing winds and downwind land determines how much moisture is exported, recycled domestically, or lost to the ocean. Net virtual water exchange depends on the socioeconomic drivers of trade, including distance [37], which shape both trade partners and the amount of blue water embedded in traded crops.

Although governance frameworks for green water are still in development [41, 42], compound metrics that combine socioeconomic trade facilitators with atmospheric moisture recycling could support decision-making from global to local scales, particularly cooperation between neighboring countries. Future work could test whether economic ties, such as trade agreements or shared borders, modulate attenuation across distance classes and whether similar patterns hold for terrestrial transboundary flows [43], and could extend the bilateral, irrigation-specific comparison introduced here to second-order and cascading connections [26, 27].

Our estimates rely on irrigated areas for 2015 from MIRCA-OS [44], used to update water use estimates originally based on circa-2000 irrigated areas [29, 45, 46], and on bilateral trade data in primary-crop equivalents averaged over 2008–2017 [30], for consistency with the reanalysis-reconciled annual atmospheric connections available for that period [34]. However, as irrigation keeps expanding, with half of its recent expansion occurring in already water-stressed regions [47], and as water scarcity deepens in major producing countries [48], extending this framework to updated irrigated areas and evolving global trade patterns, as well as to seasonal and sub-national scales through coupled land–atmosphere feedbacks, will be essential to track how these externalities evolve. This matters because irrigation directly redistributes water among the land surface, soil, and atmosphere, strongly controlling regional and global water balances [20]; it also alters the surface energy balance [21, 49] and can modify precipitation locally and remotely [19, 50].

Overall, by bringing together the atmospheric and trade-mediated redistribution of irrigation water, our results add a new dimension to metrics of transboundary water dependence and externalities, and provide a more complete basis for understanding the hydrological and socio-economic implications of irrigation under emerging transboundary water constraints [43, 51], for green water security, governance, and policy [41, 42, 52], and for identifying opportunities to strengthen cooperation [53].

3 Figures

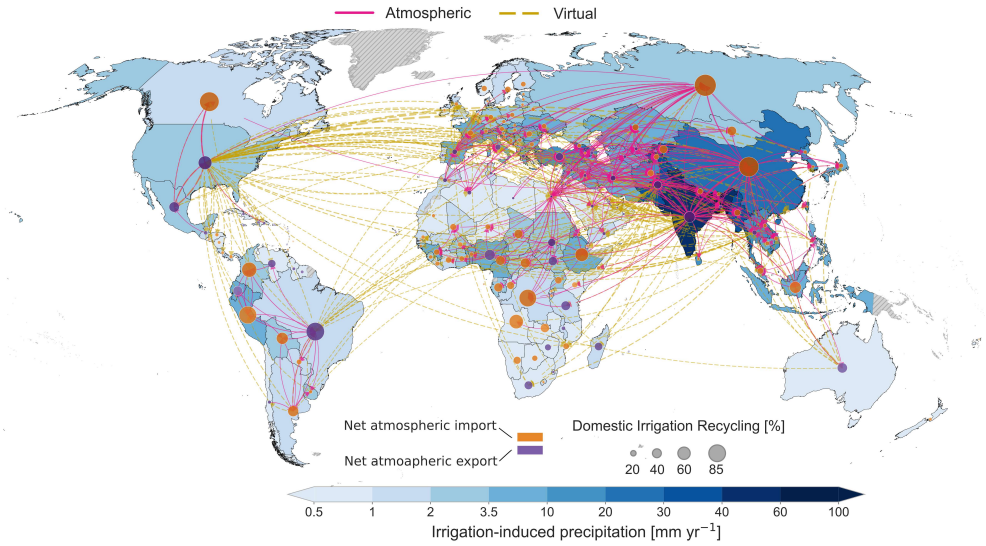


Fig. 1 Global irrigation-induced atmospheric and virtual water networks over irrigation-induced precipitation. Atmospheric (solid magenta) and virtual (dotted gold-yellow) water connections between countries originating from irrigation, with edge size proportional to flow weight. Edges represent 90% of the cumulative flows in the atmospheric network and 70% in the virtual network, around 300 connections in each network. The background layer (mm yr^{-1}) represents the annual precipitation induced by irrigation, including domestic irrigation recycling, normalized to the receiving country's area. For each country, the node color shows the net atmospheric import (orange) or export (purple) from cross-border irrigation, while node size is proportional to domestic irrigation recycling, i.e., the portion of irrigation-induced evapotranspiration that falls back as precipitation within the country's borders.

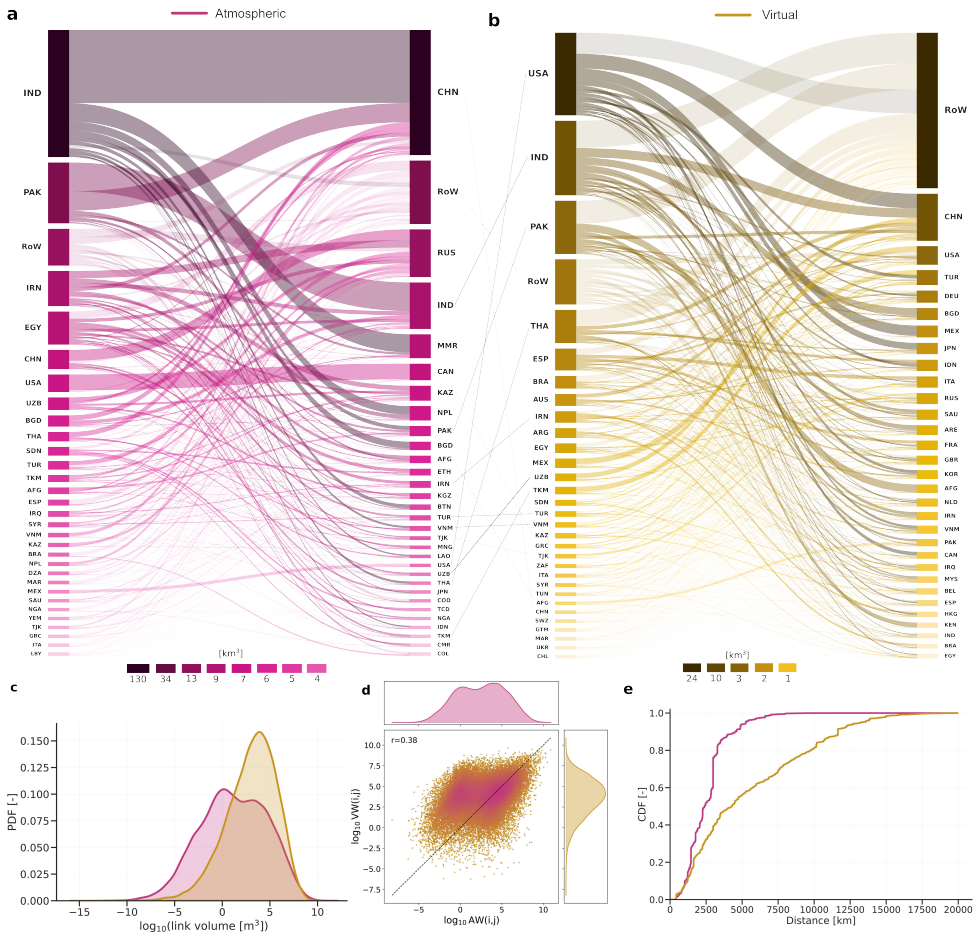


Fig. 2 Bilateral irrigation-induced atmospheric and blue virtual water flows. Sankey diagrams of global irrigation-induced **(a)** atmospheric and **(b)** blue virtual water flows between the top 30 exporters and importers and the rest of the world (RoW), in km^3 yr^{-1}. Flows are sorted in descending order and colored according to the exporting country's ranking. Lines between the panels connect each country's ranking as an atmospheric importer (a) to its ranking as a blue virtual water exporter (b): solid lines indicate a higher or equal ranking in (b), dotted lines a lower ranking. **(c)** Probability density functions of bilateral annual flows between country pairs ij (m^3; irrigation-induced atmospheric water in magenta, blue virtual water in gold). **(d)** Normalized density (0–1) of atmospheric $AW(i,j)$ against blue virtual water $VW(i,j)$ for country pairs linked by both networks, on log scales, with marginal probability density functions; the dashed line is the 1:1 line and r is Pearson's correlation coefficient. **(e)** Cumulative share of cross-border atmospheric (magenta) and blue virtual water (gold) volumes as a function of the great-circle distance between country centroids.

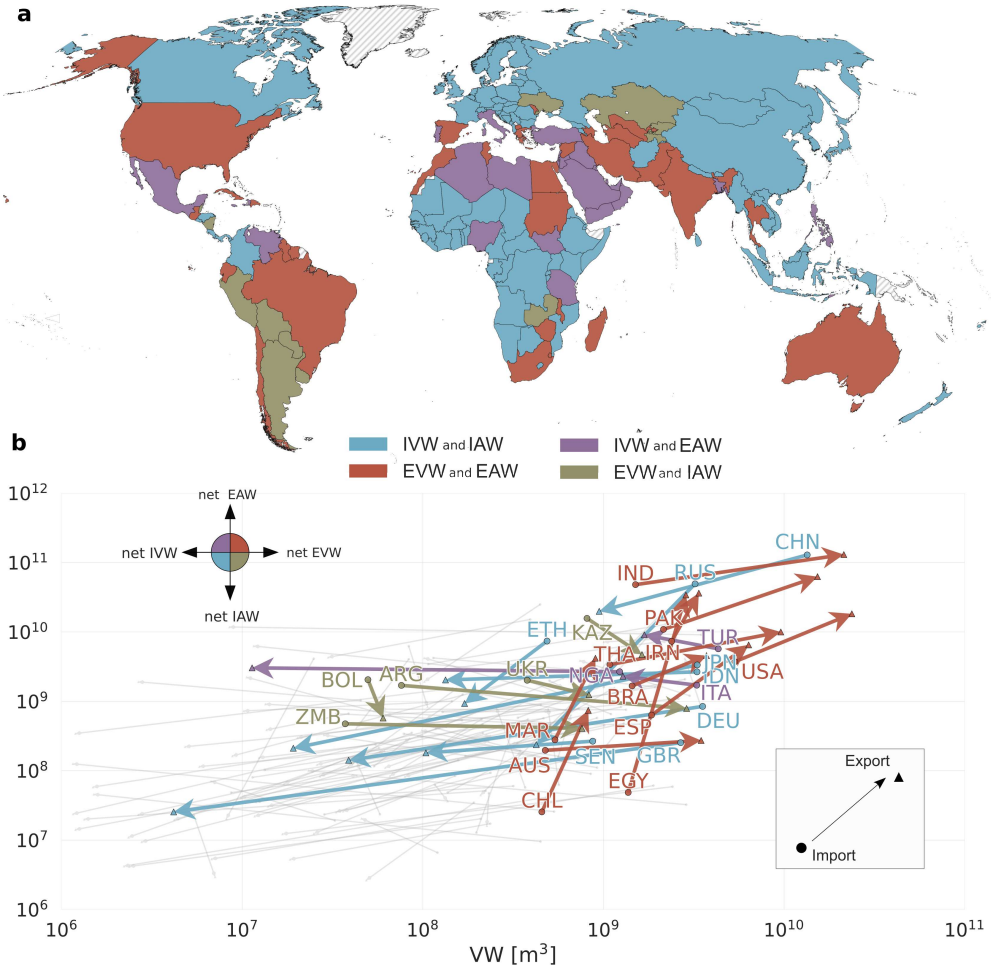


Fig. 3 Amplification and attenuation of countries' roles between the irrigation-induced atmospheric and blue virtual water trade networks. (a) Countries are colored according to their net role in the two networks: light blue, net importers in both (IVW&IAW); brick red, net exporters in both (EVW&EAW); purple, net importers of blue virtual water but net exporters of irrigation-induced atmospheric water (IVW&EAW); olive, the reverse (EVW&IAW). **(b)** Imported (IVW, IAW; circles) and exported (EVW, EAW; triangles) volumes of blue virtual water (x-axis) and irrigation-induced atmospheric water (y-axis), on log scales. IAW and EAW are cross-border irrigation-induced precipitation received and moisture exported, both excluding domestic irrigation recycling; IVW and EVW are blue virtual water imports and exports. For each country, an arrow connects the import point to the export point: it points upward when the country is a net atmospheric exporter ($EAW > IAW$) and rightward when it is a net virtual water exporter ($EVW > IVW$), and its color follows panel (a). Steeper arrows indicate that exports and imports differ more, in relative terms, in the atmospheric network than in trade; shallower arrows indicate the opposite (legend, top left). Only selected countries are labeled and colored; all other countries with both VW and AW volumes above 10^6 m^3 are shown in light grey.

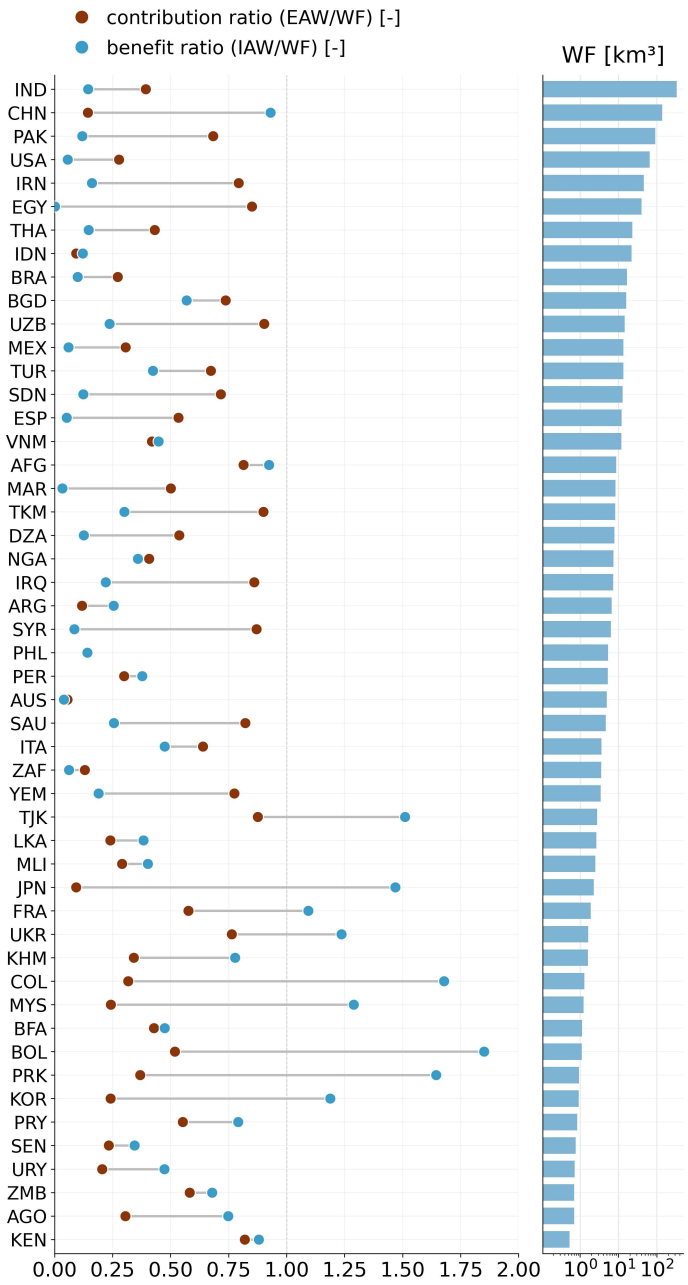


Fig. 4 Dumbbell plot of cross-border irrigation-induced benefit and contribution ratios. The contribution ratio (EAW/WF_b) and the benefit ratio (IAW/WF_b) (i.e., exported and imported irrigation-induced atmospheric flow, each normalized by the national WF_b of agricultural production). The plot shows the top 25 countries by WF_b of agricultural production with higher EAW and the top 25 countries by WF_b with higher IAW. The vertical line at $x = 1$ marks the threshold where EAW or IAW equals the national WF_b. IAW excludes domestic moisture recycling. The bars below show the WF_b (km^3) for each country on a logarithmic scale.

4 Methods

4.1 Country mapping for nomenclatures and order

We develop a country map reconciling the different nomenclatures used across the datasets in this study (i.e., CWASI, FAOSTAT, Natural Earth) to homogenize country order and identifiers before the study's main analyses. Country and ocean boundaries follow the delineations and the fractional mask protocol developed in [54, 55], applied throughout this study to assign gridded irrigation, evapotranspiration, and atmospheric moisture data to the country scale. All countries with a non-zero WF_b are retained in the global volumes and in the bilateral matrices. Country-level indicators (roles, ratios, medians and shares) are computed for countries with $WF_b \geq 10^6$ m^3 yr^{-1}, since ratios normalized by very small WF_b values—totaling 0.003 km^3–(Antigua and Barbuda, Liberia, Ireland, Trinidad and Tobago, Hong Kong, Estonia, Barbados, São Tomé and Príncipe, Saint Kitts and Nevis, Luxembourg, Macao, Saint Lucia) are dominated by the resolution of the input data; Puerto Rico, which has no bilateral trade record of food trade, is also excluded, leaving 162 irrigated countries in both networks.

4.2 Crop-specific irrigation-induced evapotranspiration volume

Actual irrigated areas are sourced from the up-to-date, crop-specific irrigation dataset MIRCA-OS [44], built from national and sub-national census and statistical data for the year 2015. MIRCA-OS updates and refines the widely used MIRCA2000 baseline [45], centered on 1996–2005; validated against independent census and gridded products, it shows good overall spatial agreement with MIRCA2000, particularly across core breadbasket regions, with the largest differences attributable to the more refined, higher-resolution harvested-area statistics now available for underrepresented regions and crops [44]. All gridded crop data (23 crop classes, equivalent to the 26 classes of the original MIRCA2000 dataset [45]) are provided at 0.5° resolution and are summed and masked to the country scale as described above. Because irrigation occurs only on land, in coastal cells the fractional country weights are rescaled by their sum over the countries present in the cell, so that no irrigated area is attributed to the sea; the same rule is applied to MIRCA2000 and MIRCA-OS before computing the ratio in Eq. 1.

To evaluate crop-specific irrigation-induced evapotranspiration, we refer to the blue crop water footprint of production (CWF_b), which measures the amount of water required in each country to produce one unit of a primary product (expressed in m^3 t^{-1}) from surface water and groundwater bodies. The CWF_b is the output of the agro-hydrological evaluation of crop actual evapotranspiration based on the water-CROP model [28], coupling a daily soil water balance with FAO-56 crop coefficients [56] to simulate irrigation requirements and evapotranspiration for 148 crops at high spatial resolution (5 arc minutes); the model's own global sensitivity analysis identifies the climate input dataset and the assumed crop calendar as the dominant sources of uncertainty, ahead of soil parameters and the effective-precipitation method [28], and

waterCROP-derived estimates are directly benchmarked against independent datasets [48, 57].

Temporal variability in CWF_b is captured through the fast-track (FT) method [46], which uses the WaterStat database [58] to express spatial variation in evapotranspiration and the ratio of agricultural yields to express its temporal variability, information not detailed in WaterStat itself. The FT method keeps actual crop evapotranspiration implicitly constant at the long-term WaterStat average; this is justified because yield already reflects the combined effect of climatic conditions, water availability, soil fertility, and agricultural practices, so that temporal yield variations dominate the variability of crop water use, while CWF_b—being a ratio of evapotranspiration to yield, both of which respond with the same sign to hydro-climatic fluctuations—is comparatively less sensitive to these fluctuations than evapotranspiration alone [59]. Additional detail on the uncertainty of the FT method is given in [29, 46]. For each crop c and year t, CWF_b is sourced from the updated CWASI database v1.4 built on this rationale [30].

However, the FT approach implemented in CWASI relies on stable, 1996–2005-centered irrigated areas from MIRCA2000 [45]. To account for the temporal evolution of irrigated areas, we update the underlying irrigated area to 2015 using MIRCA-OS [44], following the rescaling approach of [60], where the updated $CWF'_b(i,c,t)$ is obtained by scaling the original CWASI estimate $CWF_b(i,c,t)$ by the ratio of MIRCA-OS to MIRCA2000 irrigated area in country i,

$$CWF'_b(i,c,t) = \frac{A_{\mathrm{I,MIRCA\text{-}OS}}(i)}{A_{\mathrm{I,MIRCA2000}}(i)} \cdot CWF_b(i,c,t) \quad [\mathrm{m^3\ t^{-1}}] \tag{1}$$

This approach may introduce uncertainty; however, it is justified by the rationale of holding yields constant across irrigated areas.

Then, the time-averaged updated blue crop water footprint over the period 2008–2017 ($T_a = 10$ years) is:

$$\overline{CWF'_b}(i,c) = \frac{1}{T_a} \sum_{t=1}^{T_a} CWF'_b(i,c,t) \quad [\mathrm{m^3\ t^{-1}}] \tag{2}$$

Crop-specific production $P(i,c,t)$ (in metric tons) refers to FAOSTAT [61] and is sourced from CWASI v1.4 [30] for country i, crop c, and year t, and its time-averaged value is:

$$\overline{P}(i,c) = \frac{1}{T_a} \sum_{t=1}^{T_a} P(i,c,t) \quad [\mathrm{t}] \tag{3}$$

Finally, the total WF_b of production for country i and crop c is:

$$\overline{WF_b}(i,c) = \overline{CWF'_b}(i,c) \cdot \overline{P}(i,c) \quad [\mathrm{m^3}] \tag{4}$$

and the country-level total, summed over all 148 primary crops, is:

$$\overline{WF_b}(i) = \sum_{c=1}^{148} \overline{WF_b}(i,c) \quad [\mathrm{m^3}] \tag{5}$$

$\overline{WF_b}(i)$ represents the actual evapotranspiration volume originating from the irrigation of 148 primary crops (as defined by FAOSTAT [61]) for country i, averaged over 2008–2017 and accounting for irrigated areas updated to 2015. Our global estimate of 1,052 $km^3\ yr^{-1}$ falls within the range of previous global estimates (882–1,530 $km^3\ yr^{-1}$; Supplementary Information Table 2).

4.3 Irrigation-induced bilateral atmospheric moisture matrix

Atmospheric moisture data are sourced from the RECON dataset [31], an updated, reconciled version of the UTrack database [33] generated by the Lagrangian moisture-tracking model UTrack [32]. UTrack takes advantage of state-of-the-art climate reanalysis data [62] and, by testing several combinations of model assumptions, optimally generates highly detailed evaporation footprints while avoiding unnecessary complexity; nonetheless, model error and assumptions, together with possible discrepancies in reanalysis data, can lead to inconsistencies that impede an internally consistent description of the global hydrological cycle [32, 34, 63]. RECON addresses this limitation through a reconciliation framework based on Iterative Proportional Fitting (IPF), a rigorous mathematical procedure for refining tracking-model outputs that reduces uncertainties from modeling assumptions and data resolution constraints, and further pre-processes the ERA5 reanalysis data to correct the existing annual imbalance between ERA5 precipitation and evaporation [62]. The resulting reconciliation ensures that total tracked atmospheric moisture matches total precipitation at the sink and total evaporation at the source on an annual basis, in each cell. RECON provides global coverage at 0.5° resolution on an annual basis, representing mean conditions over 2008–2017 [34]; this annual, decade-averaged scale limits the analysis of inter- and intra-annual variability in atmospheric moisture connections, but provides robust estimates at a manageable data volume (63 GB on disk), reducing computational constraints. Cell-scale data are aggregated to the country scale (267 countries and 10 ocean geographical units) following the fractional mask protocol described above [54, 55], with country- and ocean-scale outputs publicly available.

Let $\mathcal{K}$ denote the set of all destination regions, including countries and oceans, and $\mathcal{C} \subset \mathcal{K}$ the set of countries. The total land evaporation of country i, directed to both land and ocean, is obtained by summing the total atmospheric flow $AW_t(i,k)$ over all destination regions $k \in \mathcal{K}$:

$$EAW_t(i) = \sum_{k \in \mathcal{K}} AW_t(i,k) \quad [\mathrm{m}^3] \tag{6}$$

Irrigation-induced atmospheric water flows are obtained by considering the contribution of the WF_b of primary crops $\overline{WF_b}(i)$ (Eq. 5) to the total actual evaporation from land at the country scale. To do so, a scaling factor $\alpha(i)$ is calculated as the ratio of WF_b to total land evaporation:

$$\alpha(i) = \frac{\overline{WF_b}(i)}{EAW_t(i)} \quad [-] \tag{7}$$

The irrigation-induced atmospheric water flow from country i to each destination region k, including oceans, is then:

$$AW_b(i,k) = \alpha(i) \cdot AW_t(i,k) \quad [\mathrm{m}^3] \tag{8}$$

To focus on terrestrial atmospheric connections, we restrict the destinations to countries, $j \in \mathcal{C}$, and reorder it accordingly to the country mapping defined in subsection 4.1: $AW_b(i,j)$ is the matrix of irrigation-induced atmospheric moisture flows from country i to country j, whose diagonal $AW_b(i,i)$ is the domestic irrigation recycling.

4.4 Irrigation-induced bilateral virtual water trade matrix

To reconnect producer countries with final destination countries, bilateral country-scale origin-to-destination trade data quantify the volumes (in metric tons) of both primary and secondary products (expressed as primary equivalent) traded between the country of production i and the country of consumption j, covering 255 countries over 1986–2023 [64]. These declarations are reconciled between exporting and importing country pairs ij via the methodology based on [29, 65], and traced from producer to final consumer country through the NETFLOW algorithm [66], a nested algorithm that processes production vectors and reconciled bilateral trade matrices to trace primary crop origins across hierarchical levels of the supply chain, avoiding re-export and multi-layer trading issues for both primary and derived products, building on and extending the reconstruction tool of [67]. This approach tracks the origin of goods through the supply chain, yielding robust estimates of the water embedded in bilateral trade and reliable totals of virtual water in final consumption. The reconciled crop-specific trade matrix is available for all 148 primary crops considered in this study over 2008–2017, the same period over which the atmospheric moisture network is averaged (see above) [33, 34].

The crop-specific trade matrix, time-averaged over 2008–2017, is:

$$\overline{T}(i,j,c) = \frac{1}{T_a} \sum_{t=1}^{T_a} T(i,j,c,t) \quad [\mathrm{tons}] \tag{9}$$

The bilateral matrix of irrigation-induced virtual water (i.e., blue virtual water) trade for each crop c, connecting the WF_b of production to the final consumption country, is obtained by scaling each row i of the trade matrix $\overline{T}(i,j,c)$ by the corresponding country- and crop-specific water footprint $\overline{CWF'_b}(i,c)$, which varies along the producer dimension only:

$$\overline{VW_b}(i,j,c) = \overline{CWF'_b}(i,c) \cdot \overline{T}(i,j,c) \quad [\mathrm{m}^3] \tag{10}$$

where $\overline{VW_b}(i,j,c)$ and $\overline{T}(i,j,c)$ are the $N \times N$ matrices of irrigation-induced virtual water trade and production trade for crop c, with N the total number of countries.

The resulting production trade matrix aggregated over all crops is:

$$\overline{T}(i,j) = \sum_{c=1}^{148} \overline{T}(i,j,c) \quad [\mathrm{tons}] \tag{11}$$

and the total blue virtual water trade matrix is:

$$\overline{VW_b}(i,j) = \sum_{c=1}^{148} \overline{VW_b}(i,j,c) \quad [\mathrm{m}^3] \tag{12}$$

Also $\overline{VW_b}(i,j)$ is reordered accordingly to the country mapping defined in subsection 4.1

4.5 Country-scale import and export volumes of irrigation-induced virtual and atmospheric water

Total exports and imports of irrigation-induced virtual water, $EVW(i)$ and $IVW(i)$, and of atmospheric water, $EAW(i)$ and $IAW(i)$, for country i are obtained as:

$$EVW(i) = \sum_{j \neq i} \overline{VW_b}(i,j) \qquad \text{and} \qquad IVW(i) = \sum_{j \neq i} \overline{VW_b}(j,i) \quad [\mathrm{m}^3] \tag{13}$$

$$EAW(i) = \sum_{j \neq i} AW_b(i,j) \qquad \text{and} \qquad IAW(i) = \sum_{j \neq i} AW_b(j,i) \quad [\mathrm{m}^3] \tag{14}$$

To evaluate the intensity of atmospheric import and export as a depth of precipitation or evaporation, the total atmospheric import $IAW(i)$ is referred to the country area $A(i)$, sourced from the most recent FAO country-level land use records [68]:

$$iaw(i) = \frac{IAW(i)}{A(i)} \quad [\mathrm{mm}] \tag{15}$$

The previous relationship (Eq. 15) assumes that atmospheric water imports are distributed uniformly across each country's area. Clearly, this does not reflect the geographical complexity of precipitation patterns, particularly in larger countries, but it provides an intuitive representation of the magnitude of irrigation-induced water quantities transferred between countries. In reality, the local contribution of blue water—as irrigation-induced evaporation—to precipitation may vary heterogeneously within a country.

The total atmospheric export $EAW(i)$ is normalized by the irrigated area $A_I(i)$ of the sourcing country i, yielding the irrigation-induced evapotranspiration depth per unit irrigated land:

$$eaw(i) = \frac{EAW(i)}{A_I(i)} \quad [\mathrm{mm}] \tag{16}$$

4.6 Country-scale domestic irrigation recycling

For each country i, the volume of irrigation-induced evapotranspiration that precipitates back within the country's own borders is given by the diagonal of the bilateral atmospheric matrix $AW_b(i,j)$:

$$AW_b(i,i) = \mathrm{diag}(AW_b(i,j)) \quad [\mathrm{m}^3] \tag{17}$$

The domestic irrigation recycling $DIR(i)$ is defined as the fraction of the national WF_b that returns as precipitation within the same country:

$$DIR(i) = \frac{AW_b(i,i)}{\overline{WF_b}(i)} \times 100 \quad [\%] \tag{18}$$

4.7 Countries' weights in the network

The country-specific irrigation-induced atmospheric and virtual water weights of each country i, $w_{aw}(i)$ and $w_{vw}(i)$, are evaluated as the total export and import flow of the country, normalized by the total exchange volume of the entire atmospheric and virtual network (Fig.Extended Data 10):

$$w_{aw}(i) = \frac{EAW(i) + IAW(i)}{\sum_i \sum_{j \neq i} AW_b(i,j)} \times 100 \quad [\%] \tag{19}$$

and:

$$w_{vw}(i) = \frac{EVW(i) + IVW(i)}{\sum_i \sum_{j \neq i} \overline{VW_b}(i,j)} \times 100 \quad [\%] \tag{20}$$

4.8 Relative contributions to countries' total WF_b of agricultural production

The atmospheric export $EAW(i)$ and import $IAW(i)$ of each country (excluding DIR) are normalized by the national WF_b of agricultural production $WF_b(i)$, yielding dimensionless fractions that quantify, respectively, the relative contribution of irrigation-induced evapotranspiration to moisture exported to other countries, and the relative role of irrigation-sourced precipitation received from transboundary sources (Fig.4, Fig.Extended Data 9):

$$\varepsilon(i) = \frac{EAW(i)}{\overline{WF_b}(i)} \qquad \text{and} \qquad \psi(i) = \frac{IAW(i)}{\overline{WF_b}(i)} \quad [-] \tag{21}$$

where $\varepsilon(i) \in [0,1]$, while $\psi(i) > 1$ indicates that country i imports more irrigation-induced precipitation volume from cross-border countries than its total WF_b of production. $\varepsilon(i)$ is also referred to as the contribution ratio of country i, and $\psi(i)$ as the benefit ratio of country i.

4.9 Geographical analysis of country-scale atmospheric and virtual flows

A geographical coordinate $C(i)$ is assigned to each country, identified by the geometric centroid of its territory and expressed as a pair of latitude and longitude coordinates $[\text{lat}(i), \text{lon}(i)]$ in decimal degrees, converted to $[\phi(i), \lambda(i)]$ in radians. To ensure consistency between the virtual water and atmospheric flow networks, geographic centroids are used to locate each country i in both the $VW_b(i,j)$ and $AW_b(i,j)$ networks.

The great-circle distance between each pair of countries (i,j) is computed via the Haversine formula:

$$d(i,j) = 2R \arcsin\left(\sqrt{\sin^2\left(\frac{\phi(j)-\phi(i)}{2}\right) + \cos\phi(i)\cos\phi(j)\sin^2\left(\frac{\lambda(j)-\lambda(i)}{2}\right)}\right) \quad \text{[km]} \tag{22}$$

where $R = 6371$ km is the mean radius of the Earth.

The flow-weighted average global distance is computed separately for each network, excluding domestic flows ($i = j$):

$$\hat{d}_{AW} = \frac{\sum_{i \neq j} d(i,j) \cdot AW_b(i,j)}{\sum_{i \neq j} AW_b(i,j)}, \qquad \hat{d}_{VW} = \frac{\sum_{i \neq j} d(i,j) \cdot VW_b(i,j)}{\sum_{i \neq j} VW_b(i,j)} \quad \text{[km]} \tag{23}$$

4.10 Bilateral analysis of country-scale atmospheric and virtual flows

In order to compare flows $VW_b(i,j)$ and $AW_b(i,j)$, they are normalized to the respective global totals:

$$VW_g = \sum_{i,j} VW_b(i,j) \qquad \text{and} \qquad AW_g = \sum_{i,j} AW_b(i,j) \quad [\mathrm{m}^3] \tag{24}$$

where VW_g and AW_g denote the global sums of all blue virtual water and atmospheric flows, respectively.

Then, the normalized matrices are:

$$vw(i,j) = \frac{VW_b(i,j)}{VW_g} \qquad \text{and} \qquad aw(i,j) = \frac{AW_b(i,j)}{AW_g} \quad [-] \tag{25}$$

Thus, $vw(i,j)$ and $aw(i,j)$ express the share of irrigation-induced virtual water and atmospheric moisture flow, respectively, from country i to country j relative to the global total.

Their ratio over the concordant link ij is computed as:

$$r(i,j) = \frac{vw(i,j)}{aw(i,j)} \tag{26}$$

while the ratio over the atmospheric link ij and bilateral virtual water link ji is computed as:

$$r'(i,j) = \frac{vw(j,i)}{aw(i,j)} \tag{27}$$

4.11 Use of generative AI tools

The authors acknowledge using Claude (Opus 5.5, accessed in 2026) to refine the manuscript structure, review and organize the data, and debug, optimize, and clean the code.

All AI-generated suggestions were reviewed, revised, and approved by the authors, who take full responsibility for the accuracy and integrity of the work. The authors reviewed, tested, and revised all AI-generated code, confirming the accuracy and reproducibility of the results.

Acknowledgements

The authors acknowledge support from the European Research Council (ERC) through the TIP-FRESH project (grant number 101222767).

Competing interests

The authors declare no competing interests.

Data availability

All input datasets are from publicly available sources.

Crop-category actual irrigated areas are available for the year 2000 from the MIRCA2000 database https://www.geo.uni-frankfurt.de/45218031/Data_download_center_for_MIRCA2000, and from MIRCA-OS for the year 2000 and 2015 at https://www.hydroshare.org/resource/60a890eb841c460192c03bb590687145/. The RECON dataset provides moisture flow volumes in cubic meters from evaporation sources to precipitation sinks at 0.5° resolution for 2008–2017 and aligns with ERA5 reanalysis data; it is available at 10.5281/zenodo.14191919. The 3D Fractional Region Mask for aggregating global gridded data to country-scale data based on Natural Earth delineation is available at https://doi.org/10.5281/zenodo.19007673. Crop water use (CWF) and water footprint (WF_b) are available at https://doi.org/10.5281/zenodo.18964006; production values and origin-destination matrix of trade in primary equivalent are available at https://doi.org/10.5281/zenodo.23494383.

The data generated in this study are publicly available at https://doi.org/10.5281/zenodo.22876958

Code availability

The codes developed for the analyses and to generate the results can be downloaded from https://zenodo.org/uploads/22876958

Author contributions

E.D.P., M.T., L.R., and F.L. designed the study. E.D.P. conducted the analyses and produced the figures. E.D.P., M.T., L.R., and F.L. contributed to interpreting the data. E.D.P. wrote the paper. E.D.P., M.T., L.R., and F.L. edited the paper.

Figure Legends

Figure 1

Global irrigation-induced atmospheric and blue virtual water networks over irrigation-induced precipitation. Atmospheric (solid magenta) and virtual (dotted gold-yellow) water connections between countries originating from irrigation, with edge size proportional to flow weight. Edges represent 90% of the cumulative flows in the atmospheric network and 70% in the virtual network, around 300 connections in each network. The background layer (mm yr^{-1}) represents the annual precipitation induced by irrigation, including domestic irrigation recycling, normalized to the receiving country's area. For each country, the node color shows the net atmospheric import (orange) or export (purple) generated by cross-border irrigation, while node size is proportional to domestic irrigation recycling, i.e., the portion of irrigation-induced evapotranspiration that falls back as precipitation within the country's borders.

Figure 2

Bilateral irrigation-induced atmospheric and blue virtual water flows. Sankey diagrams of global irrigation-induced **(a)** atmospheric and **(b)** blue virtual water flows between the top 30 exporters and importers and the rest of the world (RoW), in km^3 yr^{-1}. Flows are sorted in descending order and colored according to the exporting country's ranking. Lines between the panels connect each country's ranking as an atmospheric importer (a) to its ranking as a blue virtual water exporter (b): solid lines indicate a higher or equal ranking in (b), dotted lines a lower ranking. **(c)** Probability density functions of bilateral annual flows between country pairs ij (m^3; irrigation-induced atmospheric water in magenta, blue virtual water in gold). **(d)** Normalized density (0–1) of atmospheric $AW(i,j)$ against blue virtual water $VW(i,j)$ for country pairs linked by both networks, on log scales, with marginal probability density functions; the dashed line is the 1:1 line and r is Pearson's correlation coefficient. **(e)** Cumulative share of cross-border atmospheric (magenta) and blue virtual water (gold) volumes as a function of the great-circle distance between country centroids.

Figure 3

Amplification and attenuation of countries' roles between the irrigation-induced atmospheric and blue virtual water trade networks. (a) Countries are colored according to their net role in the two networks: light blue, net importers in both (IVW&IAW); brick red, net exporters in both (EVW&EAW); purple, net importers of blue virtual water but net exporters of irrigation-induced atmospheric water (IVW&EAW); olive, the reverse (EVW&IAW). **(b)** Imported (IVW, IAW; circles) and exported (EVW, EAW; triangles) volumes of blue virtual water (x-axis) and irrigation-induced atmospheric water (y-axis), on log scales. IAW and EAW are cross-border irrigation-induced precipitation received and moisture exported, both excluding domestic irrigation recycling; IVW and EVW are blue virtual water imports and exports. For each country, an arrow connects the import point to the export point: it points upward when the country is a net atmospheric exporter ($EAW > IAW$)

and rightward when it is a net virtual water exporter ($EVW > IVW$), and its color follows panel (a). Steeper arrows indicate that exports and imports differ more, in relative terms, in the atmospheric network than in trade; shallower arrows indicate the opposite (legend, top left). Only selected countries are labeled and colored; all other countries with both VW and AW volumes above 10^6 m^3 are shown in light grey.

Figure 4

Dumbbell plot of cross-border irrigation-induced benefit and contribution ratios. The contribution ratio (EAW/WF_b) and the benefit ratio (IAW/WF_b) (i.e., exported and imported irrigation-induced atmospheric flow, each normalized by the national WF_b of agricultural production). The plot shows the top 25 countries by WF_b of agricultural production with higher EAW and the top 25 countries by WF_b with higher IAW. The vertical line at $x = 1$ marks the threshold where EAW or IAW equals the national WF_b. IAW excludes domestic moisture recycling. The bars below show the WF_b (km^3) for each country on a logarithmic scale.

References

[1] Gleeson, T., Wang-Erlandsson, L., Zipper, S.C., Porkka, M., Jaramillo, F., Gerten, D., Fetzer, I., Cornell, S.E., Piemontese, L., Gordon, L.J., *et al.*: The water planetary boundary: interrogation and revision. One Earth **2**(3), 223–234 (2020)

[2] Virkki, V., Andersen, L.S., te Wierik, S., Gerten, D., Porkka, M.: Regionally divergent drivers behind transgressions of the freshwater change planetary boundary. Nature Communications (2026)

[3] Food and Agriculture Organization of the United Nations (FAO): The State of the World's Land and Water Resources for Food and Agriculture – Systems at Breaking Point. Main Report. FAO, Rome, Italy (2022). https://doi.org/10.4060/cb9910en

[4] Kohli, A., Frenken, K., Spottorno, C.: Disambiguation of water statistics. Technical report, AQUASTAT Programme, Food and Agriculture Organization of the United Nations (FAO), Rome, Italy (2012). Revised version, 23 May 2012 (first published 23 September 2010)

[5] Gimeno, L., Vázquez, M., Eiras-Barca, J., Sorí, R., Stojanovic, M., Algarra, I., Nieto, R., Ramos, A.M., Duran-Quesada, A.M., Dominguez, F.: Recent progress on the sources of continental precipitation as revealed by moisture transport analysis. Earth-Science Reviews **201**, 103070 (2020)

[6] Falkenmark, M.: Water cycle and people: water for feeding humanity. Land Use and Water Resources Research **3**, 3–134 (2003)

[7] Ent, R.J., Savenije, H.H., Schaefli, B., Steele-Dunne, S.C.: Origin and fate of atmospheric moisture over continents. Water Resources Research **46**(9) (2010) https://doi.org/10.1029/2010WR009127

[8] De Petrillo, E., Fahrländer, S., Tuninetti, M., Andersen, L., Monaco, L., Ridolfi, L., Laio, F.: Reconciling tracked atmospheric water flows to close the global freshwater cycle. Communications Earth & Environment **6**(347) (2025) https://doi.org/10.1038/s43247-025-02289-y

[9] Allan, J.A., *et al.*: Fortunately there are substitutes for water otherwise our hydro-political futures would be impossible. Priorities for water resources allocation and management **13**(4), 26 (1993)

[10] D'Odorico, P., Carr, J., Dalin, C., Dell'Angelo, J., Konar, M., Laio, F., Ridolfi, L., Rosa, L., Suweis, S., Tamea, S., Tuninetti, M.: Global virtual water trade and the hydrological cycle: patterns, drivers, and socio-environmental impacts. Environmental Research Letters **14**, 053001 (2019) https://doi.org/10.1088/1748-9326/ab05f4

[11] D'Odorico, P., Carr, J.A., Laio, F., Ridolfi, L., Vandoni, S.: Feeding humanity through global food trade. Earth's Future **2**(9), 458–469 (2014)

[12] Food and Agriculture Organization of the United Nations (FAO): The State of Agricultural Commodity Markets 2022. The Geography of Food and Agricultural Trade: Policy Approaches for Sustainable Development. FAO, Rome, Italy (2022). https://doi.org/10.4060/cc0471en

[13] Dalin, C., Wada, Y., Kastner, T., Puma, M.J.: Groundwater depletion embedded in international food trade. Nature **543**(7647), 700–704 (2017)

[14] Rosa, L., Chiarelli, D.D., Tu, C., Rulli, M.C., D'Odorico, P.: Global unsustainable virtual water flows in agricultural trade. Environmental Research Letters **14**(11), 114001 (2019)

[15] Vallino, E., Ridolfi, L., Laio, F.: Trade of economically and physically scarce virtual water in the global food network. Scientific Reports **11**(1), 22806 (2021)

[16] Mekonnen, M.M., Kebede, M.M., Demeke, B.W., Carr, J.A., Chapagain, A., Dalin, C., Debaere, P., D'Odorico, P., Marston, L., Ray, C., Rosa, L., Zhuo, L.: Trends and environmental impacts of virtual water trade. Nature Reviews Earth & Environment **5**, 890–905 (2024) https://doi.org/10.1038/s43017-024-00605-2

[17] Gu, W., Wang, F., Siebert, S., Kummu, M., Wang, X., Hong, C., Zhou, F., Zhu, Q., Liu, Y., Qin, Y.: The asymmetric impacts of international agricultural trade on water use scarcity, inequality and inequity. Nature Water **2**(4), 324–336 (2024)

[18] Wei, J., Dirmeyer, P.A., Wisser, D., Bosilovich, M.G., Mocko, D.M.: Where Does

the Irrigation Water Go? An Estimate of the Contribution of Irrigation to Precipitation Using MERRA. Journal of Hydrometeorology **14**(1), 275–289 (2013) https://doi.org/10.1175/JHM-D-12-079.1

[19] Vrese, P., Hagemann, S., Claussen, M.: Asian irrigation, african rain: Remote impacts of irrigation. Geophysical Research Letters **43**(8), 3737–3745 (2016)

[20] McDermid, S., Nocco, M., Lawston-Parker, P., Keune, J., Pokhrel, Y., Jain, M., Jägermeyr, J., Brocca, L., Massari, C., Jones, A.D., Vahmani, P., Thiery, W., Yao, Y., Bell, A., Chen, L., Dorigo, W., Hanasaki, N., Jasechko, S., Lo, M.-H., Mahmood, R., Mishra, V., Mueller, N.D., Niyogi, D., Rabin, S.S., Sloat, L., Wada, Y., Zappa, L., Chen, F., Cook, B.I., Kim, H., Lombardozzi, D., Polcher, J., Ryu, D., Santanello, J., Satoh, Y., Seneviratne, S., Singh, D., Yokohata, T.: Irrigation in the Earth system. Nature Reviews Earth & Environment **4**(7), 435–453 (2023) https://doi.org/10.1038/s43017-023-00438-5

[21] Greve, P., Schmitt, A.U., Miralles, D.G., McDermid, S., Findell, K.L., García-García, A., Peng, J.: Observational evidence of increased afternoon rainfall downwind of irrigated areas. Nature Communications **16**, 3415 (2025) https://doi.org/10.1038/s41467-025-58729-y

[22] Koppa, A., Bassani, F., Keune, J., Deman, V., Insua-Costa, D., Hari, V., Ghosh, S., Miralles, D.G., Bonetti, S.: Irrigated agriculture supports rainfed crops in India through atmospheric moisture recycling. Environmental Research Letters **21**, 104037 (2026) https://doi.org/10.1088/1748-9326/ae6f34

[23] Berger, M., Ent, R., Eisner, S., Bach, V., Finkbeiner, M.: Water Accounting and Vulnerability Evaluation (WAVE): Considering Atmospheric Evaporation Recycling and the Risk of Freshwater Depletion in Water Footprinting. Environ. Sci. Technol. **48**(8), 4521–4528 (2014) https://doi.org/10.1021/es404994t

[24] Berger, M., Eisner, S., Ent, R., Flörke, M., Link, A., Poligkeit, J., Bach, V., Finkbeiner, M.: Enhancing the Water Accounting and Vulnerability Evaluation Model: WAVE+. Environ. Sci. Technol. **52**(18), 10757–10766 (2018) https://doi.org/10.1021/acs.est.7b05164

[25] Keune, J., Miralles, D.: A precipitation recycling network to assess freshwater vulnerability: Challenging the watershed convention. Water Resources Research **55**(11), 9947–9961 (2019)

[26] Pranindita, A., Teuling, A.J., Fetzer, I., Wang-Erlandsson, L.: Forests support global crop supply through atmospheric moisture transport. Nature Water **3**(11), 1243–1255 (2025)

[27] Fahrländer, S., Lotcheris, R., Andersen, L., Gerten, D., Donges, J., Tuninetti, M., Staal, A., Wang-Erlandsson, L., Rockström, J., Wunderling, N.: Coupled atmospheric moisture and trade networks reveal a concentration of global freshwater

risk in a handful of countries. Preprint (2026)

[28] Tuninetti, M., Tamea, S., D'Odorico, P., Laio, F., Ridolfi, L.: Global sensitivity of high-resolution estimates of crop water footprint. Water Resources Research **51**(10), 8257–8272 (2015)

[29] Tamea, S., Tuninetti, M., Soligno, I., Laio, F.: Virtual water trade and water footprint of agricultural goods: the 1961–2016 CWASI database. Earth System Science Data **13**(5), 2025–2051 (2021) https://doi.org/10.5194/essd-13-2025-2021

[30] Tamea, S., Tuninetti, M., Semeria, F., Giordano, V., De Petrillo, E., Laio, F.: CWASI database: virtual water trade and water footprint of agricultural products (1961-2023). Zenodo (2026). https://doi.org/10.5281/zenodo.18964006

[31] De Petrillo, E., Monaco, L., Tuninetti, M., Staal, A., Laio, F.: RECON - Cell-scale atmospheric moisture flows dataset reconciled with ERA5 reanalysis. Zenodo (2025). https://doi.org/10.5281/zenodo.17633702

[32] Tuinenburg, O.A., Staal, A.: Tracking the global flows of atmospheric moisture and associated uncertainties. Hydrol. Earth Syst. Sci. **24**(5), 2419–2435 (2020) https://doi.org/10.5194/hess-24-2419-2020

[33] Tuinenburg, O.A., Theeuwen, J.J.E., Staal, A.: High-resolution global atmospheric moisture connections from evaporation to precipitation. Earth Syst. Sci. Data **12**(4), 3177–3188 (2020) https://doi.org/10.5194/essd-12-3177-2020

[34] De Petrillo, E., Monaco, L., Tuninetti, M., Staal, A., Laio, F.: Cell-scale atmospheric moisture flows dataset reconciled with ERA5 reanalysis. Scientific Data **12**(1), 629 (2025)

[35] Jägerskog, A., Lundqvist, J.: Water wars, conflict and cooperation–how the virtual water concept helped change the discourse. Water International **47**(6), 901–904 (2022)

[36] Graham, N.T., Hejazi, M.I., Kim, S.H., Davies, E.G., Edmonds, J.A., Miralles-Wilhelm, F.: Future changes in the trading of virtual water. Nature Communications **11**(1), 1–7 (2020)

[37] Tamea, S., Carr, J., Laio, F., Ridolfi, L.: Drivers of the virtual water trade. Water Resources Research **50**(1), 17–28 (2014)

[38] Falsetti, B., Ridolfi, L., Laio, F.: Role of trade agreements in the global cereal market and implications for virtual water flows. Scientific Reports **12**(1), 6790 (2022)

[39] Kim, D., Steinbach, S., Zurita, C.: Virtual water trade and economic integration: The role of trade agreements in global water redistribution. Applied Economic

Perspectives and Policy **47**(5), 1998–2018 (2025) https://doi.org/10.1002/aepp.70021 https://onlinelibrary.wiley.com/doi/pdf/10.1002/aepp.70021

[40] UN-Water: Transboundary waters: Sharing benefits, sharing responsibilities. Technical report, United Nations (2008)

[41] Keys, P.W., Wang-Erlandsson, L., Gordon, L.J., Galaz, V., Ebbesson, J.: Approaching moisture recycling governance. Global Environmental Change **45**, 15–23 (2017)

[42] te Wierik, S.A., Gupta, J., Cammeraat, E.L., Artzy-Randrup, Y.A.: The need for green and atmospheric water governance. Wiley Interdisciplinary Reviews: Water **7**(2), 1406 (2020)

[43] Munia, H., Guillaume, J., Mirumachi, N., Porkka, M., Wada, Y., Kummu, M.: Water stress in global transboundary river basins: significance of upstream water use on downstream stress. Environmental Research Letters **11**(1), 014002 (2016)

[44] Kebede, E.A., Oluoch, K.O., Siebert, S., Mehta, P., Hartman, S., Jägermeyr, J., Ray, D., Ali, T., Brauman, K.A., Deng, Q., *et al.*: A global open-source dataset of monthly irrigated and rainfed cropped areas (MIRCA-OS) for the 21st century. Scientific Data **12**(1), 208 (2025)

[45] Portmann, F.T., Siebert, S., Döll, P.: MIRCA2000—global monthly irrigated and rainfed crop areas around the year 2000: A new high-resolution data set for agricultural and hydrological modeling. Global Biogeochemical Cycles **24**(1) (2010)

[46] Tuninetti, M., Tamea, S., Laio, F., Ridolfi, L.: A fast track approach to deal with the temporal dimension of crop water footprint. Environmental Research Letters **12**(7), 074010 (2017)

[47] Mehta, P., Siebert, S., Kummu, M., Deng, Q., Ali, T., Marston, L., Xie, W., Davis, K.F.: Half of twenty-first century global irrigation expansion has been in water-stressed regions. Nature Water **2**(3), 254–261 (2024) https://doi.org/10.1038/s44221-024-00206-9

[48] Deng, Q., Sharretts, T., Ali, T., Ao, Y.Z., Chiarelli, D.D., Demeke, B., Marston, L., Mehta, P., Mekonnen, M., Rulli, M.C., Tuninetti, M., Xie, W., Davis, K.F.: Deepening water scarcity in breadbasket nations. Nature Communications **16**(1), 1110 (2025) https://doi.org/10.1038/s41467-025-56022-6

[49] Thiery, W., Davin, E.L., Lawrence, D.M., Hirsch, A.L., Hauser, M., Seneviratne, S.I.: Present-day irrigation mitigates heat extremes. Journal of Geophysical Research: Atmospheres **122**(3), 1403–1422 (2017) https://doi.org/10.1002/2016JD025740

[50] Fan, Y., Yang, Z., Lo, M.-H., Hur, J., Im, E.-S.: Deciphering the capricious precipitation response: irrigation impact in the North China Plain. npj Climate and Atmospheric Science **8**, 211 (2025) https://doi.org/10.1038/s41612-025-01063-3

[51] Madani, K.: Global water bankruptcy: Living beyond our hydrological means in the post-crisis era. Technical report, United Nations University Institute for Water, Environment and Health (UNU-INWEH), Richmond Hill, Ontario, Canada (2026). https://doi.org/10.53328/INR26KAM001

[52] Posada-Marín, J., Salazar, J., Rulli, M.C., Wang-Erlandsson, L., Jaramillo, F.: Upwind moisture supply increases risk to water security. Nature Water **2**(9), 875–888 (2024)

[53] Borgomeo, E., Loske-Garcia, L., Leb, C.: Moisture in motion: Integrating green water in transboundary water governance and development finance-a guidance note for transboundary waters practitioners (2026)

[54] De Petrillo, E., Fahrländer, S.F., Tuninetti, M., Andersen, L.S., Monaco, L., Thomas, R.F., Cigna, G., Ridolfi, L., Laio, F.: Country-ocean-moisture-flows-reconciled-with-ERA5-reanalysis obtained processing Lagrangian moisture connections. Zenodo (2026). https://doi.org/10.5281/zenodo.19101962

[55] Thomas, R.F., Cigna, G., De Petrillo, E.: 3D Fractional Region Mask for Aggregating Global Gridded Data. Zenodo (2026). https://doi.org/10.5281/zenodo.19007673

[56] Allen, R.G., Pereira, L.S., Raes, D., Smith, M.: Crop evapotranspiration: Guidelines for computing crop water requirements. FAO Irrigation and Drainage Paper 56, FAO, Rome (1998)

[57] De Petrillo, E., Tuninetti, M., Ridolfi, L., Laio, F.: International corporations trading Brazilian soy are keystone actors for water stewardship. Communications Earth & Environment **4**, 87 (2023) https://doi.org/10.1038/s43247-023-00742-4

[58] Mekonnen, M.M., Hoekstra, A.Y.: The green, blue and grey water footprint of crops and derived crop products. Hydrology and Earth System Sciences **15**(5), 1577–1600 (2011) https://doi.org/10.5194/hess-15-1577-2011

[59] Doorenbos, J., Kassam, A.H., Bentvelsen, C.L.M., Branscheid, V., Plusjé, J.M.G.A., Smith, M., Uittenbogaard, G.O., Van Der Wal, H.K.: Yield response to water. FAO Irrigation and Drainage Paper 33, FAO, Rome (1979)

[60] Tuninetti, M., Tamea, S., Dalin, C.: Water debt indicator reveals where agricultural water use exceeds sustainable levels. Water Resources Research **55**(3), 2464–2477 (2019)

[61] FAOSTAT: Crop Production. http://www.fao.org/faostat/en/#data/QC

[62] Hersbach, H., Bell, B., Berrisford, P., Hirahara, S., Horányi, A., Muñoz-Sabater, J., Nicolas, J., Peubey, C., Radu, R., Schepers, D., *et al.*: The ERA5 global reanalysis. Quarterly Journal of the Royal Meteorological Society **146**(730), 1999–2049 (2020)

[63] Giordano, V., Ridolfi, L., Staal, A., Tuninetti, M., Laio, F.: Novel validation and performance assessment framework for atmospheric moisture tracking approaches: The case of UTrack. Under review (2026)

[64] Semeria, F., De Petrillo, E., Laio, F., Tamea, S., Tuninetti, M.: Origin–destination Trade Matrices for Agricultural Products at the Country Scale over the Period 1986–2023. https://doi.org/10.5281/zenodo.23494383 . https://doi.org/10.5281/zenodo.23494383

[65] Distefano, T., Tuninetti, M., Laio, F., Ridolfi, L.: Tools for reconstructing the bilateral trade network: a critical assessment. Economic Systems Research **32**, 378–394 (2020) https://doi.org/10.1080/09535314.2019.1703173

[66] Semeria, F., Ridolfi, L., Tuninetti, M.: A multi-level network tool to trace wasted water from farm to fork and backwards. Environmental Research Letters **19**(7), 074026 (2024)

[67] Kastner, T., Kastner, M., Nonhebel, S.: Tracing distant environmental impacts of agricultural products from a consumer perspective. Ecological Economics **70**(6), 1032–1040 (2011)

[68] FAO: Land statistics 2001–2023 – global, regional and country trends. Technical Report 107, Food and Agriculture Organization of the United Nations, Rome (2025)

Extended Data

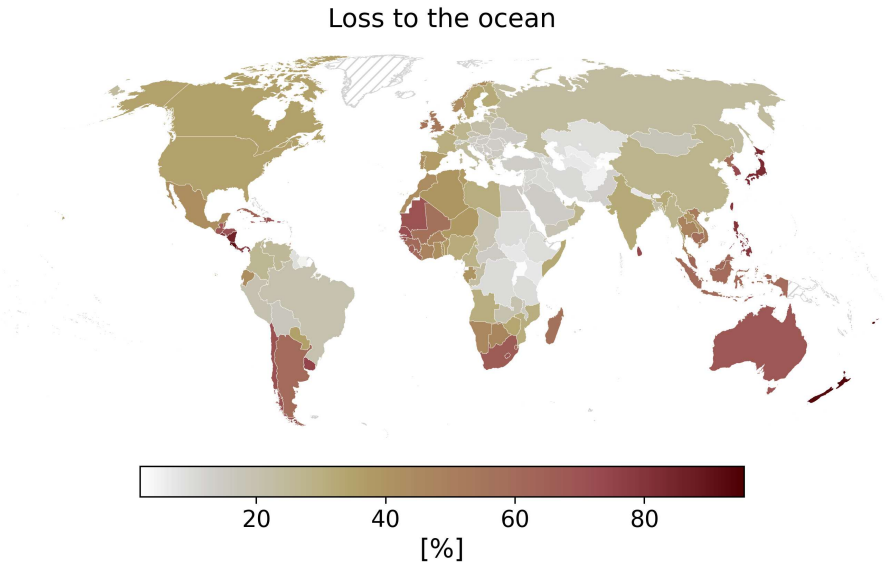


Fig. Extended Data 1 Country-scale loss to the ocean, defined as the share of the national WF_b (irrigation-induced evapotranspiration) transported over and precipitating on the ocean rather than returning as precipitation over land.

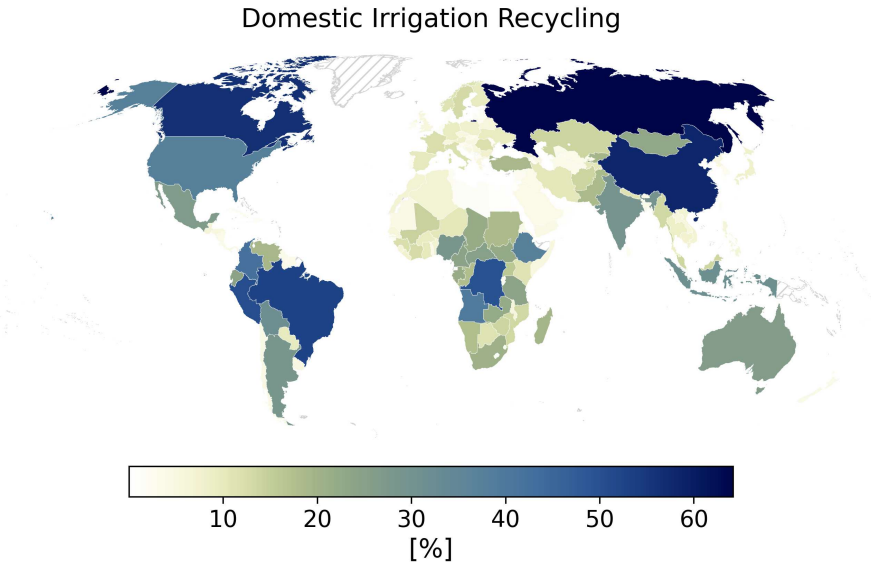


Fig. Extended Data 2 Country-scale domestic irrigation recycling (DIR, Eq. 18), defined as the share of irrigation-induced evapotranspiration (the WF_b of agricultural production) that returns as precipitation within the country of origin.

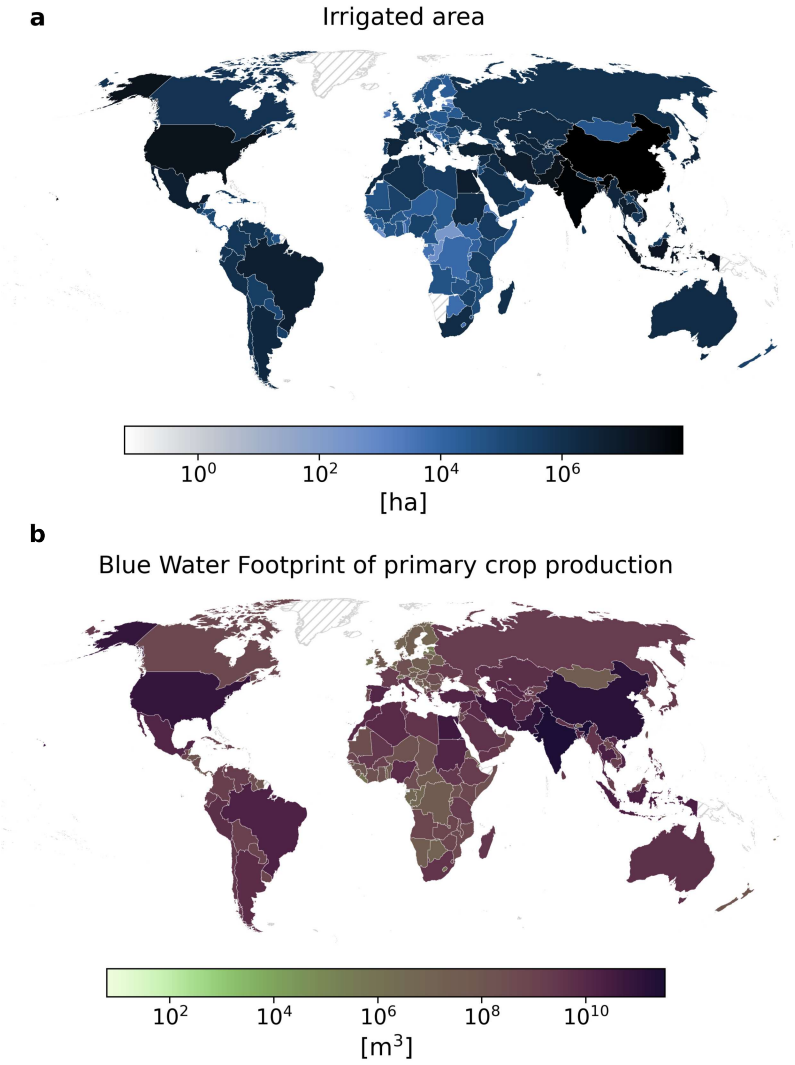


Fig. Extended Data 3 Country-scale **(a)** harvested irrigated area (ha), derived from the pixel-level MIRCA-OS dataset for 2015 [44], and **(b)** WF_b of primary crop production, evaluated as an updated version of the CWASI database [29, 30, 46]. Missing data are shown with a hatched pattern.

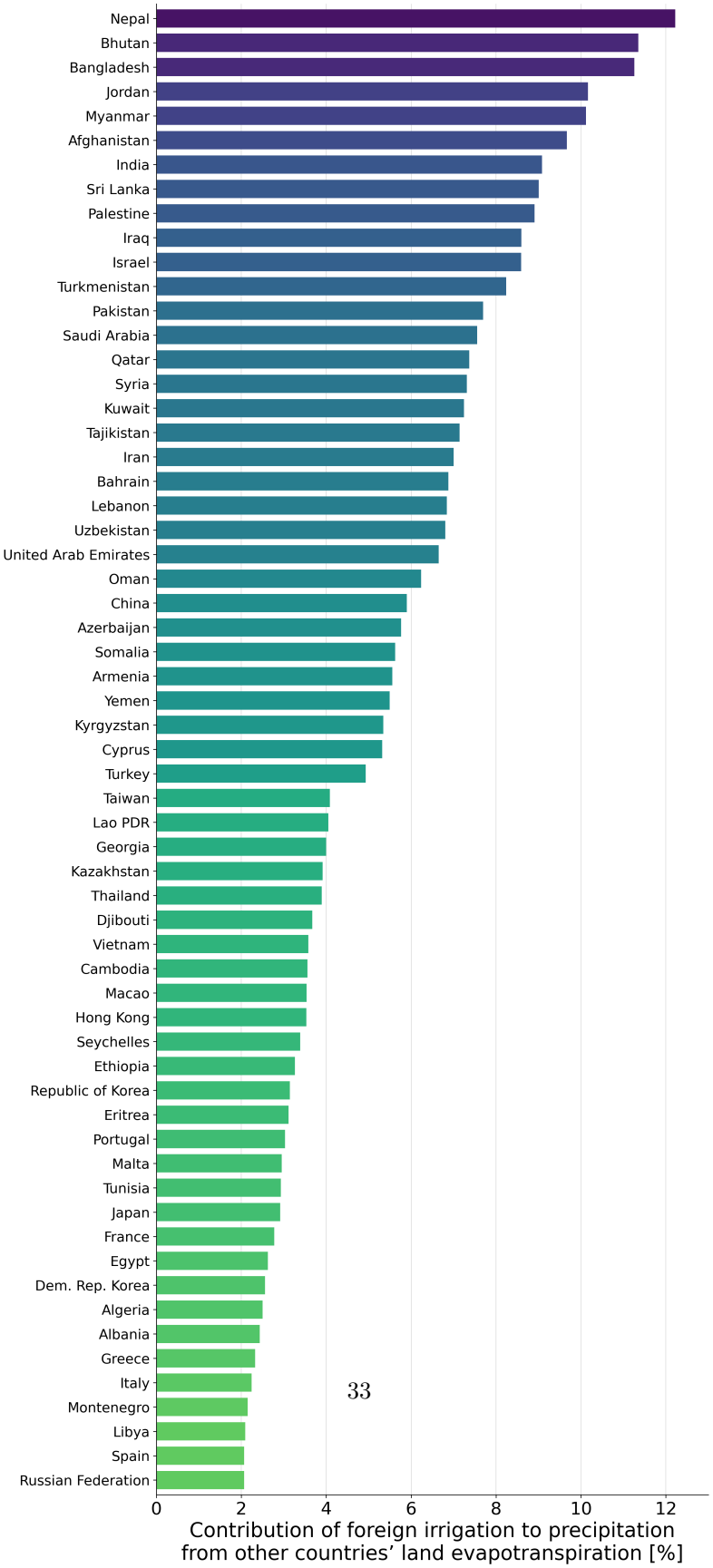


Fig. Extended Data 4 Contribution of foreign irrigation-induced evapotranspiration to the precipitation falling within each country's borders, expressed as a percentage of the total precipitation originating from land evapotranspiration in other countries. Only countries with a contribution of at least 2% are shown.

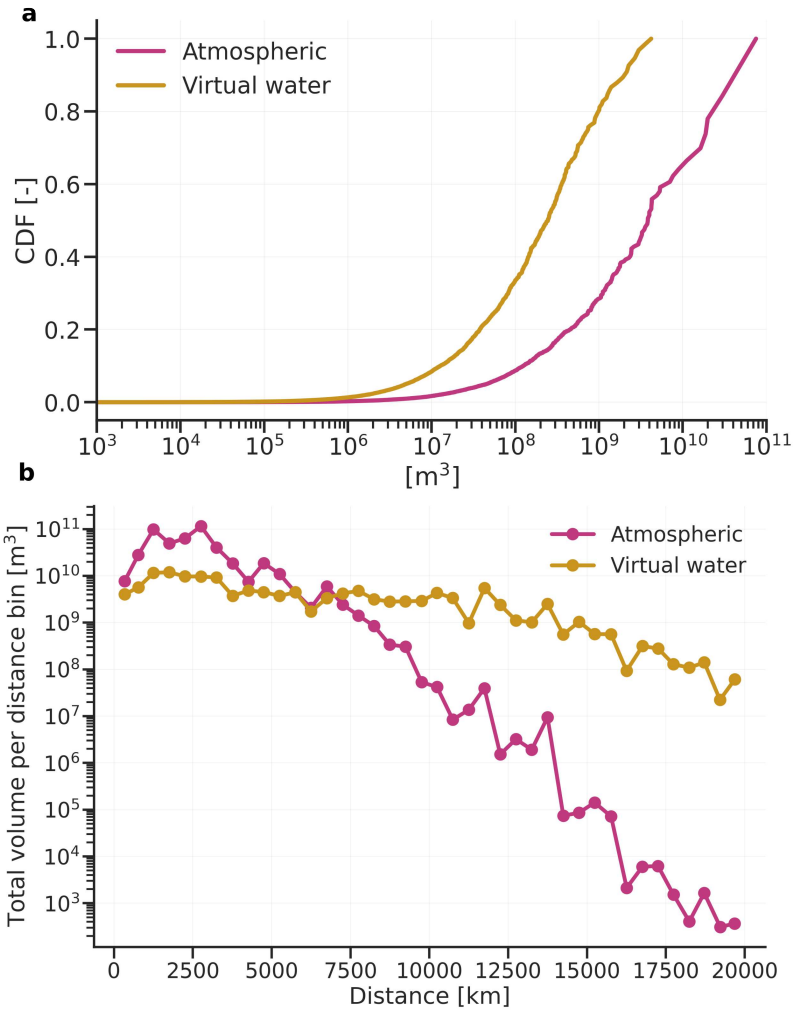


Fig. Extended Data 5 Bilateral analysis of volumes and distances across links of the irrigation-induced atmospheric and blue virtual water networks. **(a)** Weighted cumulative density function of atmospheric (magenta) and virtual (gold) water flows between countries i and j originating from cross-border irrigated agricultural production. The cumulative frequency is weighted by the bilateral atmospheric (virtual) water flow between countries i and j. The x-axis is on a log scale. **(b)** Relationship between distance (km, x-axis) and the magnitude of the bilateral link (m^3, y-axis, log scale).

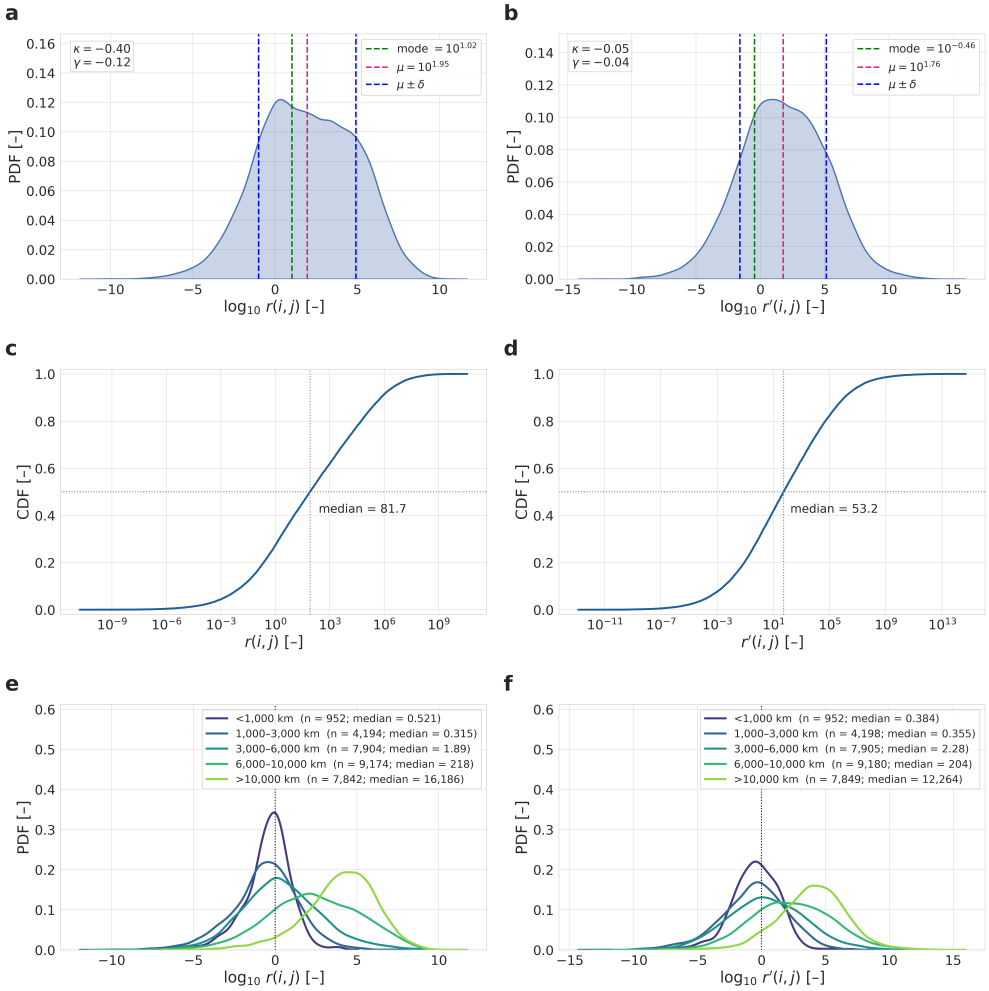


Fig. Extended Data 6 The probability density functions are shown for **(a)** $r(i,j)$, which is calculated as the ratio of the normalized bilateral flows $vw(i,j)$ and $aw(i,j)$ (see Eq. 26), and **(b)** $r'(i,j)$, which is calculated as the ratio of the normalized bilateral flows $vw(j,i)$ and $aw(i,j)$ (see Eq. 27). The plots also show the mode (green dotted line), mean (magenta dotted line), standard deviation (blue dotted line), and kurtosis (κ) and skewness (γ) of the distribution. Panels **(c)** and **(d)** show the cumulative density functions of $r(i,j)$ and $r'(i,j)$, respectively, over the total number of bilateral links, while panels **(e)** and **(f)** show the probability density functions by distance classes (colors).

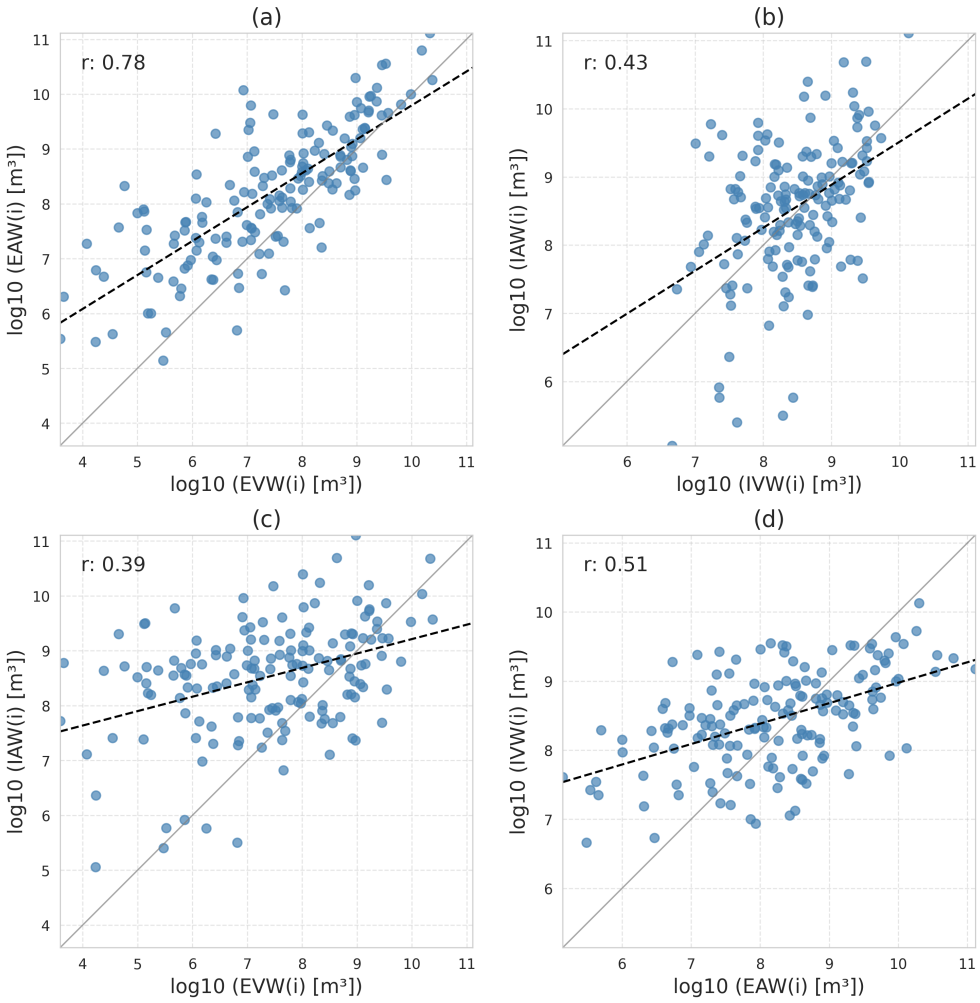


Fig. Extended Data 7 Scatterplots of country-scale volumes (m^3) of **(a)** exported virtual water (x-axis) and exported atmospheric water (i.e., irrigation-induced evapotranspiration; y-axis); **(b)** imported virtual water (x-axis) and imported atmospheric water (i.e., irrigation-induced precipitation; y-axis); **(c)** exported virtual water (x-axis) and imported atmospheric water (y-axis); **(d)** exported atmospheric water (x-axis) and imported virtual water (y-axis). Atmospheric water excludes domestic irrigation recycling. Axes are on a log scale.

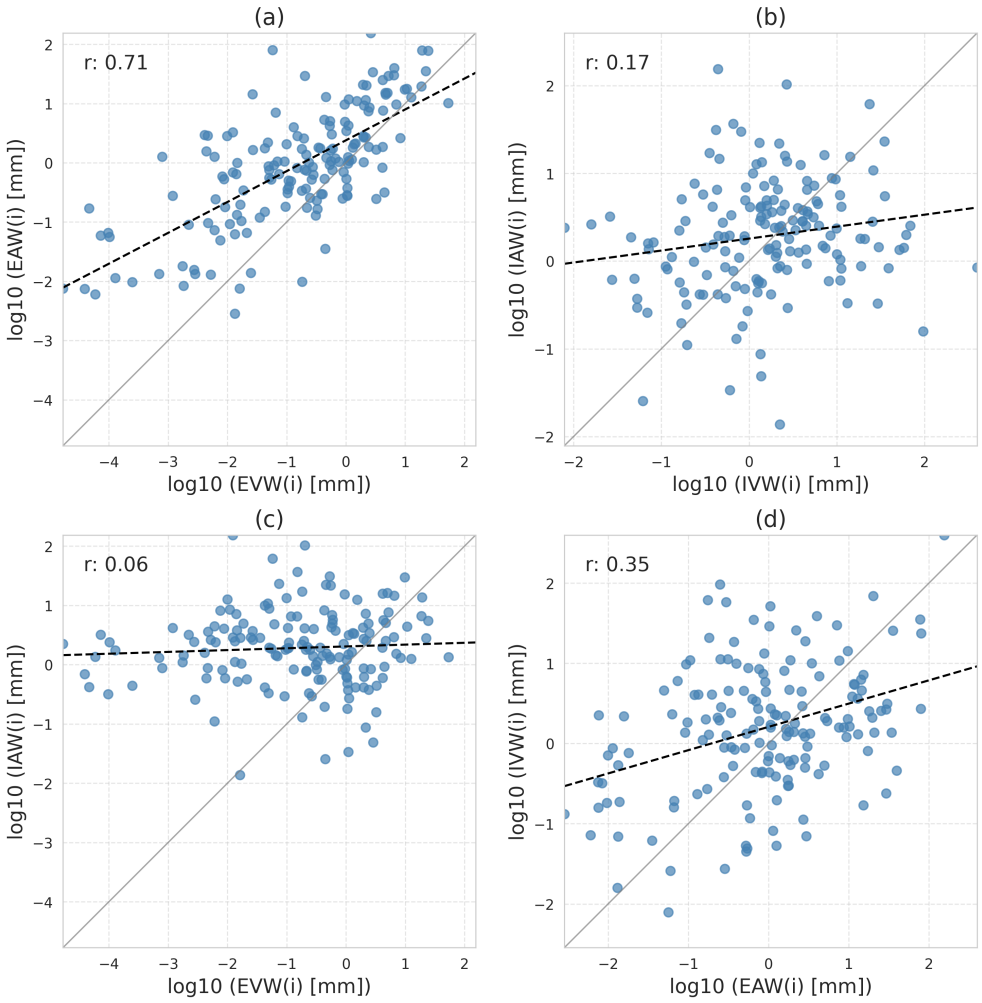


Fig. Extended Data 8 Scatterplots of country-scale precipitation heights (mm) obtained by normalizing volumes by country area. **(a)** exported virtual water (x-axis) and exported atmospheric water (i.e., irrigation-induced evapotranspiration; y-axis); **(b)** imported virtual water (x-axis) and imported atmospheric water (i.e., irrigation-induced precipitation; y-axis); **(c)** exported virtual water (x-axis) and imported atmospheric water (y-axis); **(d)** exported atmospheric water (x-axis) and imported virtual water (y-axis). Atmospheric water excludes domestic irrigation recycling.

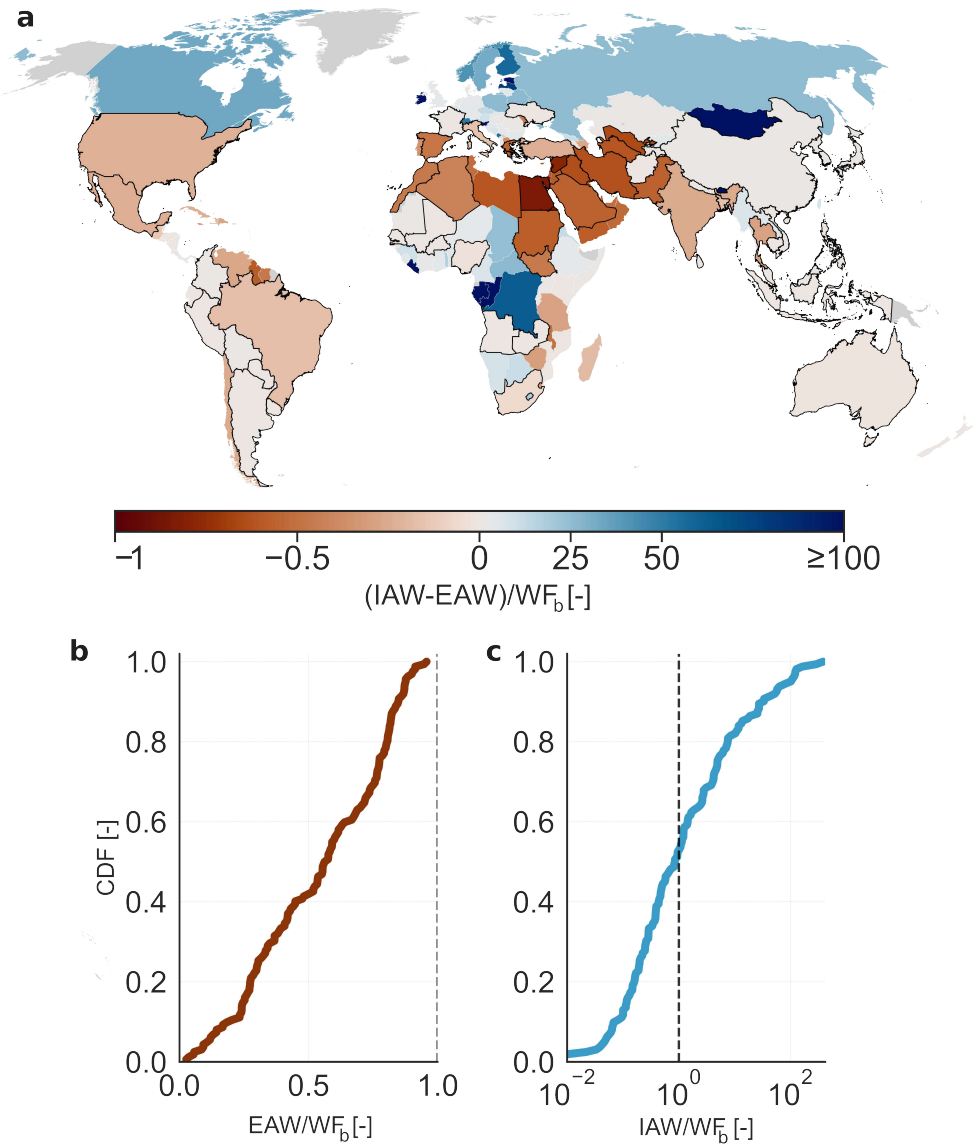


Fig. Extended Data 9 (a) Map of the net normalized atmospheric balance at the country scale, $(IAW - EAW)/WF_b$, i.e., the difference between the benefit and contribution ratios (IAW and EAW exclude domestic irrigation recycling). Shades of red indicate net atmospheric exporters (values < 0; the minimum is -1 when the entire WF_b is exported), while shades of blue indicate net atmospheric importers (values > 0); values above 100 are shown in the darkest blue. Countries shown in Fig. 4 are outlined in black. (b, c) Cumulative distribution functions of (b) the contribution ratio EAW/WF_b and (c) the benefit ratio IAW/WF_b (log scale) across the 162 irrigated countries; the dashed line marks a ratio of 1, where EAW or IAW equals the national WF_b.

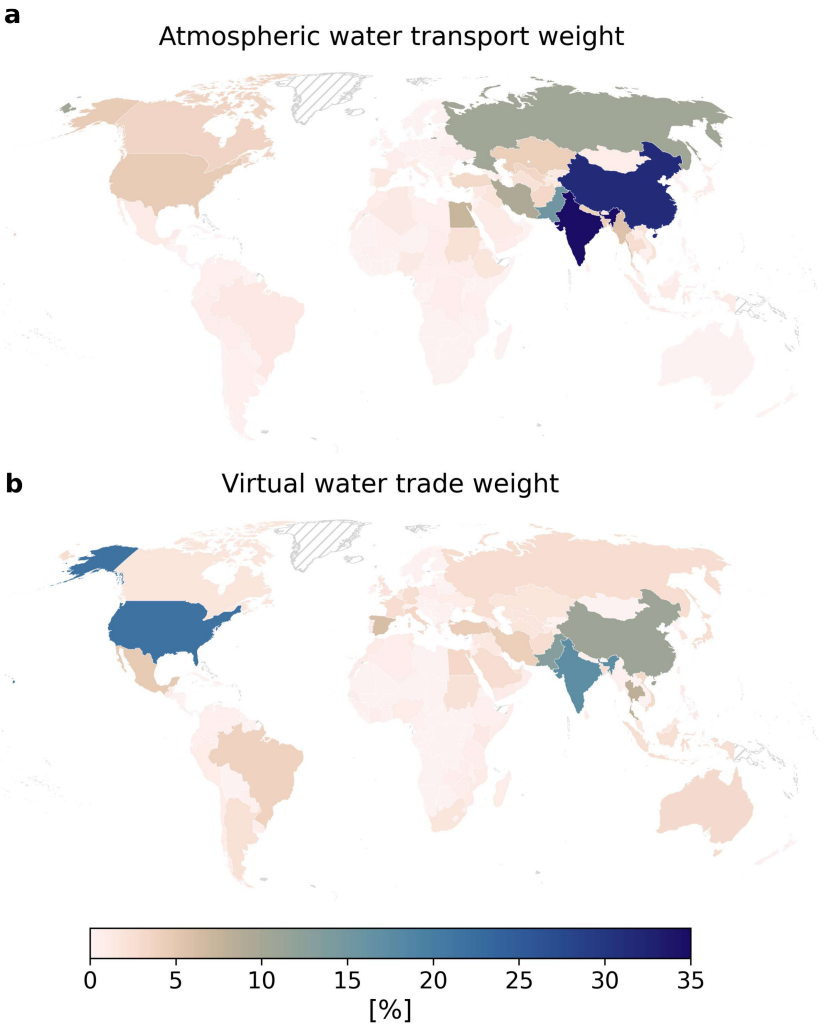


Fig. Extended Data 10 Country-scale weight in the **(a)** atmospheric moisture network and **(b)** virtual water network, both supported by irrigation-induced evapotranspiration only (Eqs. 19–20). Each country's weight is computed as the sum of its cross-border imports and exports, normalized by the total volume of transboundary water flows exchanged globally.

Supplementary Files

This is a list of supplementary files associated with this preprint. Click to download.

- SupplementaryInformation.pdf